Collocating Volatility

A Competitive Alternative to Stochastic Local Volatility Models

van der Stoep, Anthonie W.; Grzelak, Lech A.; Oosterlee, Cornelis W.

DOI
10.1142/S0219024920500387

Publication date
2020

Document Version
Accepted author manuscript

Published in
International Journal of Theoretical and Applied Finance

Collocating Local Volatility: A Competitive Alternative to Stochastic Local Volatility Models

Anthonie W. van der Stoep[a,b,c,*] Lech A. Grzelak[c,d]
Cornelis W. Oosterlee[a,c]

Version: June 4, 2018

Abstract

We discuss a competitive alternative to stochastic local volatility models, namely the *Collocating Local Volatility* (CLV) model, introduced in [21]. The CLV model consists of two elements, a 'kernel process' which can be efficiently evaluated and a local volatility function. The latter, based on stochastic collocation [2, 16, 39, 40, 40], connects the kernel process to the market and allows the CLV model to be perfectly calibrated to European-type options. In this article we consider three different kernel process choices: the Ornstein-Uhlenbeck (OU) and Cox-Ingersoll-Ross (CIR) processes and the Heston model. The kernel process controls the forward smile and allows for an accurate and efficient calibration to exotic options, while the perfect calibration to liquid market quotes is preserved. We confirm this by numerical experiments, in which we calibrate the OU-CLV, CIR-CLV and Heston-CLV models to FX barrier options.

Keywords: Collocating Local Volatility, stochastic local volatility, Monte Carlo, stochastic collocation, calibration, forward volatility, barrier options.

1 Introduction

In the last decade, the class of *stochastic local volatility* (SLV) models – e.g. [9, 26, 27, 31, 33, 36, 37] – has been given a lot of attention. According to Lipton et al., SLV models are the *de facto* standard for pricing FX options in practice [28]. They combine the desirable features of the standard Local Volatility model [10, 12] – an almost perfect calibration to liquid European-type options – and well-established stochastic volatility models such as the Heston model [24] and the SABR model [23], which often yield realistic forward smiles and prices of exotics. However, SLV models involve some conditional expectation that is non-trivial and may be expensive to evaluate.

In this article we consider an alternative to SLV models, namely the *Collocating Local Volatility* (CLV) model, introduced in [21]. The CLV model is composed of a kernel process and a local volatility function, which is constructed based on stochastic collocation [2, 5, 30, 35, 40] and, as a consequence, admits a perfect calibration to arbitrage-free European-type option prices. The kernel process can be *any* stochastic process – in the case however that the moments of the kernel variable exist and are numerically stable, optimal collocation points can be determined by which the local volatility function is defined [20].

The CLV model allows for flexibility regarding the forward smile. The forward smile is governed by the kernel process and reflects the transition densities between future states of

[a]CWI - National Research Institute for Mathematics and Computer Science, Amsterdam, the Netherlands.
[b]Pricing Model Validation, Rabobank, Utrecht, the Netherlands.
[c]Delft Institute of Applied Mathematics, Delft University of Technology, Delft, the Netherlands.
[d]Financial Engineering, Rabobank, Utrecht, the Netherlands.
[*]Corresponding author. E-mail address: Anton.van.der.Stoep@rabobank.com.

the underlying, which determine the price of a path-dependent product [3]. By an appropriate choice of the kernel process and its parameter values, the CLV model is well-capable of pricing exotic options, while maintaining a fit to liquid European-style options. In this article we consider three different kernel processes: the Ornstein-Uhlenbeck (OU) and Cox-Ingersoll-Ross (CIR) processes and the Heston model.

Another advantageous property of the CLV model is the fact that the local volatility function only needs to be evaluated at the time-points of interest. In addition, the kernel process typically allows for large time-steps in a simulation. This particularly holds if an analytical solution is available (as for e.g. the OU and CIR kernel processes), however also for other processes efficient simulation schemes exist, e.g. the Heston model can be efficiently simulated by Andersen's QE scheme [1].

The CLV model, by its flexibility in controlling the forward smile and its rapid Monte Carlo evaluation, allows for an efficient Monte Carlo calibration to exotic options, while the fit to European-type options is preserved.

The present article is organized as follows. In Section 2 we present the CLV model and elaborate on its advantageous properties. We establish the corresponding pricing PDE along the lines of the derivation of the Black-Scholes pricing PDE – we employ the notion of martingales. Also, for application purposes we describe the evaluation steps of the CLV model in a Monte Carlo simulation framework. Subsequently, in Section 3 we consider three choices for the kernel process, namely OU and CIR dynamics and the Heston model; we describe the characteristics and consider the effect of the kernel parameters on the shape of the forward smile. Based on this analysis, in Section 4 we calibrate the OU, CIR and Heston kernel processes to FX barrier options. Last, Section 5 concludes.

2 The Collocating Local Volatility Model

In this section we discuss the main characteristics of the Collocating Local Volatility (CLV) model [21]. Also, we write the model in a standard form and derive its pricing PDE.

The CLV model is represented by the following equations, under the risk-neutral $\mathbb{Q}$-measure:

$$S(t) = g_N(t, X(t)), \tag{2.1}$$

$$\mathrm{d}X(t) = \mu^{\mathbb{Q}}(t, X(t))\mathrm{d}t + \sigma(t, X(t))\mathrm{d}W^{\mathbb{Q}}(t),\ X(t_0) = X_0. \tag{2.2}$$

The model consists of two elements that are evaluated separately. The first building block is the *kernel process* $X(\cdot)$ in (2.2). The second building block is the CLV element (2.1), which connects the kernel process to liquid market quotes via the *local volatility function* $g_N(t, x)$, which is based on the *stochastic collocation method* [2, 5, 30, 35, 40].

An advantageous property of the CLV model is that, by construction, function $g_N(\cdot, \cdot)$ guarantees an almost perfect calibration to arbitrage-free European-type option prices, *independently of the kernel parameter values*. Basically this function, given liquid market quotes for expiries $T_1, \ldots, T_M$, yields a highly accurate interpolation through the pairs $(x_{i,j}, s_{i,j})$, $i = 1, \ldots, M,\ j = 1, \ldots, N$, with $x_{i,1}, \ldots, x_{i,N}$ and $s_{i,1}, \ldots, s_{i,N}$ representing the *collocation points* and *collocation values* corresponding to T_i, respectively. The collocation points may be established based on the moments of the kernel variable (see Remark 2.1). The collocation values are computed by

$$s_{i,j} = F^{-1}_{S(T_i)}(F_{X(T_i)}(x_{i,j})),$$

where the cumulative distribution function of $S(T_i)$ *under the risk-neutral measure* is specified by equation (2.3) in Lemma 2.1.

The function $g_N(\cdot, \cdot)$ is an interpolation through the $s_{i,j}$-values, given particular t and $X(\cdot)$ values. Choosing $g_N(\cdot, \cdot)$ in the Lagrange form is well-accepted in the field of Uncertainty Quantification, see e.g. [34]. However, this choice does not guarantee monotonicity in the

strike direction, which is a desirable property. We therefore choose a piecewise cubic Hermite interpolation, which is guaranteed to be monotonic and continuously differentiable, see e.g. [15].

Lemma 2.1 (Market-implied CDF of $S(\cdot)$ under the risk-neutral measure)**.** *The market-implied CDF of $S(T)$ under the risk-neutral $\mathbb{Q}$-measure is given by*

$$F_{S(T)}(x) = 1 + \mathrm{e}^{rT} \frac{\partial V^{\mathrm{mkt}}(T,K)}{\partial K}\bigg|_{K=x}, \tag{2.3}$$

with $V^{\mathrm{mkt}}(T,K)$ denoting today's arbitrage-free price of a European call option with strike K and expiry T and r denotes a constant interest rate.

Proof. In general, the discounted value of a standard European option with an expiry T and strike K at time t under the risk-neutral $\mathbb{Q}$-measure is

$$V(T,K) = M(t)\mathbb{E}^{\mathbb{Q}}\left[\frac{(S(T)-K)^+}{M(T)}\bigg|\mathcal{F}(t)\right],$$

where $S(\cdot)$ is the underlying and $M(\cdot)$ stands for the money account, determined by $\mathrm{d}M(t) = rM(t)\mathrm{d}t$ with a constant interest rate r. The discounted value of the option is given by (suppressing the filtration notation):

$$V(T,K) = \mathrm{e}^{-rT}\mathbb{E}^{\mathbb{Q}}\left[(S(T)-K)^+\right] = \mathrm{e}^{-rT}\int_K^\infty (x-K) f_{S(T)}(x)\mathrm{d}x, \tag{2.4}$$

where $f_{S(T)}(\cdot)$ is the market-implied PDF of $S(T)$ under the $\mathbb{Q}$-measure. Differentiating and applying Leibniz' integration rule gives

$$\mathrm{e}^{rT}\frac{\partial V(T,K)}{\partial K} = -1 + F_{S(T)}(K),$$

which we write for an arbitrary argument x as:

$$F_{S(T)}(x) = 1 + \mathrm{e}^{rT}\frac{\partial V^{\mathrm{mkt}}(T,K)}{\partial K}\bigg|_{K=x},$$

where we added the 'mkt' superscript to emphasize that we obtain the CDF from the market quotes. This concludes the proof of Lemma 2.1. □

Remark 2.1 (Optimal collocation points)**.** *Optimal collocation points $x_{i,1},\ldots,x_{i,N}$ can be calculated based on the first $2N$ moments of the underlying kernel variable at T_i, $X(T_i)$ [20]. In this case the collocation points are zeros of the orthogonal polynomial corresponding to (the probability density function of) the kernel variable and can be computed by an eigenvalue method. By choosing optimal collocation points, the stochastic collocation method can be connected to the computation of integrals by Gauss quadrature. See Appendix A for more details on optimal collocation points. In [2], in an elliptic PDE framework, a rigorous convergence analysis of the stochastic collocation method is provided, where exponential convergence with respect to the number of "Gauss points" is proven.*

Remark 2.2 (Relation between $X(t)$ and $S(t)$)**.** *Ideally, for a given t, the relation between the distribution of the kernel variable and the market-implied distribution is approximately linear or, stated differently, the densities of $X(t)$ and $S(t)$ resemble each other. This yields a small approximation error [20] and optimal results.*

Besides for its almost perfect calibration, a second beneficial property of the CLV model is the fact that, in e.g. a Monte Carlo simulation framework, we do not need to evaluate $g_N(\cdot,\cdot)$ at each time-step, which is the case for the standard Local Volatility model [11, 12].

For example, for pricing a European-type option we simulate the kernel process (2.2) up to the option's maturity T and subsequently compute $g_N(T, X(T))$ (2.1). In the case that the time-points of interest are specified on a coarse grid, we prefer a simulation method for the kernel variable which is low-biased for large time-steps[1]. Moreover, in the case that the kernel process has an analytical solution (e.g. the Ornstein-Uhlenbeck and Cox-Ingersoll-Ross processes), it allows for an *exact* simulation method with large time-steps.

A third advantageous characteristic of the CLV model is its flexibility in controlling the forward smile, while maintaining an almost perfect fit to European-type options by construction. It is a well-known property of the standard Local Volatility model that it produces a *flattening forward smile*, which may be not in line with market observations [37]. This may lead to a mispricing of products that are sensitive to the forward smile, like cliquets and barrier options. Regarding the CLV model, however, as discussed in [21], the autocorrelation of the kernel process affects the forward smile. As such, the choice of kernel process and the kernel parameter values determine the forward smile generated by the CLV model, without affecting the almost perfect calibration to European-type options. The payoff of a path-dependent product is determined by the evolution of the underlying through time, i.e. its price depends on the transition densities from one future state to another [3].

As the CLV model is flexible in controlling the forward smile and can be efficiently evaluated, it allows for an efficient Monte Carlo calibration to exotic options, while the fit to European-type options is maintained. In Section 3 we consider the forward smile for three different choices of the kernel process, and in Section 4 we calibrate the kernel process to FX barrier options.

Typically, in the field of financial engineering, the dynamics of the underlying $S(\cdot)$ are presented, as opposed to the non-standard model representation in equations (2.1)-(2.2). We however can write this model in a more standard way by applying Itô's lemma. Introducing the short-hand notation $g_N := g_N(t, X(t))$, assuming that $X(\cdot)$ is a one-dimensional kernel process and that the relevant partial derivatives $\partial g_N/\partial X$, $\partial^2 g_N/\partial X^2$ and $\partial g_N/\partial t$ exist, $S(\cdot)$ follows an Itô process which is governed by the same Wiener process as $X(\cdot)$, under the risk-neutral $\mathbb{Q}$-measure:

$$\mathrm{d}S(t) = \left(\frac{\partial g_N}{\partial t} + \mu^{\mathbb{Q}}(t, X(t)) \frac{\partial g_N}{\partial X} + \frac{1}{2} \frac{\partial^2 g_N}{\partial X^2} \sigma^2(t, X(t)) \right) \mathrm{d}t + \frac{\partial g_N}{\partial X} \sigma(t, X(t)) \mathrm{d}W^{\mathbb{Q}}(t).$$

Analogous to the derivation of the Black-Scholes pricing PDE, we derive the CLV pricing PDE. To express the PDE merely in terms of derivatives to X, we define

$$\widetilde{V}(t, X(t)) := V(t, g_N(t, X(t))) = V(t, S(t)),$$

with $V(t, S(t))$ representing the value of a European option on the underlying $S(\cdot)$ ('plain vanilla contingent claim').

Lemma 2.2 (CLV pricing PDE)**.** *Given the CLV model under the risk-neutral $\mathbb{Q}$-measure with a general one-dimensional kernel process $X(\cdot)$:*

$$\begin{aligned} S(t) &= g_N(t, X(t)), \\ \mathrm{d}X(t) &= \mu^{\mathbb{Q}}(t, X(t))\mathrm{d}t + \sigma(t, X(t))\mathrm{d}W^{\mathbb{Q}}(t). \end{aligned}$$

Suppose that the partial derivatives of $g_N := g_N(t, X(t))$, $\partial g_N/\partial X$, $\partial^2 g_N/\partial X^2$ and $\partial g_N/\partial t$ exist. Also, assume that the money account $M(\cdot)$ is determined by $\mathrm{d}M(t) = rM(t)\mathrm{d}t$, with r denoting a constant interest rate. Then $\widetilde{V} := \widetilde{V}(t, X(t))$ is governed by

$$\frac{\partial \widetilde{V}}{\partial t} + \mu^{\mathbb{Q}}(t, X) \frac{\partial \widetilde{V}}{\partial X} + \frac{1}{2} \sigma^2(t, X) \frac{\partial^2 \widetilde{V}}{\partial X^2} - r\widetilde{V} = 0, \tag{2.5}$$

[1] For example, in the case of a Heston kernel process we would simulate $X(\cdot)$ by employing the *QE scheme* of Andersen [1], which allows for large time-steps. An alternative would be to make use of the so-called *exact simulation scheme* proposed by Broadie and Kaya [6], which is based on acceptance-rejection sampling of the variance process coupled with certain Fourier inversion computations. As presented in [20], by employing the Stochastic Collocation Monte Carlo sampler the exact simulation can be performed efficiently and accurately.

with the final condition

$$\widetilde{V}(T, X(T)) = \Phi(g_N(T, X(T))),$$

where $\Phi(\cdot)$ *is a payoff function depending on the final state of* $g_N(\cdot, \cdot)$.

Proof. By Itô's lemma, introducing the short-hand notation $\widetilde{V} := \widetilde{V}(t, X(t))$, we obtain:

$$\mathrm{d}\widetilde{V}(t, X(t)) = \left(\frac{\partial \widetilde{V}}{\partial t} + \mu^{\mathbb{Q}}(t, X(t)) \frac{\partial \widetilde{V}}{\partial X} + \frac{1}{2}\sigma^2(t, X(t)) \frac{\partial^2 \widetilde{V}}{\partial X^2} \right) \mathrm{d}t + \sigma(t, X(t)) \frac{\partial \widetilde{V}}{\partial X} \mathrm{d}W^{\mathbb{Q}}(t).$$

The option value discounted by the money account is a *martingale*. Based on this, we derive the PDE followed by $\widetilde{V}(t, X(t))$. Introducing the short-hand notation

$$\Pi(t, X(t)) := \frac{\widetilde{V}(t, X(t))}{M(t)},$$

and substituting the dynamics of $M := M(t)$ and $\widetilde{V} := \widetilde{V}(t, X(t))$, the dynamics of the discounted option value are given by

$$\mathrm{d}\Pi(t, X(t)) = \frac{1}{M} \left(\frac{\partial \widetilde{V}}{\partial t} + \mu^{\mathbb{Q}}(t, X(t)) \frac{\partial \widetilde{V}}{\partial X} + \frac{1}{2}\sigma^2(t, X(t)) \frac{\partial^2 \widetilde{V}}{\partial X^2} - r\widetilde{V} \right) \mathrm{d}t + \frac{\sigma(t, X(t))}{M} \frac{\partial \widetilde{V}}{\partial X} \mathrm{d}W^{\mathbb{Q}}(t).$$

As the discounted option value, under the risk-neutral $\mathbb{Q}$-measure, is a martingale, the drift term is zero, i.e.

$$\frac{\partial \widetilde{V}}{\partial t} + \mu^{\mathbb{Q}}(t, X) \frac{\partial \widetilde{V}}{\partial X} + \frac{1}{2}\sigma^2(t, X) \frac{\partial^2 \widetilde{V}}{\partial X^2} - r\widetilde{V} = 0.$$

The final condition on $\widetilde{V}(\cdot)$ is given in terms of the payoff function $\Phi(\cdot)$ that depends on the final state of $g_N(\cdot, \cdot)$:

$$\widetilde{V}(T, X(T)) = \Phi(g_N(T, X(T))).$$

This concludes the proof of Lemma 2.2. □

The PDE (2.5) is solved backwards in time, given the condition at the time to maturity. It follows from the Feynman-Kac theorem that a solution of (2.5) at an arbitrary time $t_0 < T$ is given by

$$\frac{\widetilde{V}(t_0, X(t_0))}{M(t_0)} = \mathbb{E}^{\mathbb{Q}} \left[\frac{\Phi(g_N(T, X(T)))}{M(T)} \middle| \mathcal{F}(t_0) \right].$$

We employed the notion of martingales to prove Lemma 2.2. An alternative proof is based on a *replicating portfolio* approach, see Appendix B. We construct a portfolio that replicates a European option, i.e. the portfolio and the option produce identical cashflows. As such, assuming the absence of arbitrage, the values of the portfolio and the option must be equal. In addition, the portfolio, also referred to as the delta-hedge portfolio, changes with the same amount in value as the European option, if the underlying changes.

2.1 Martingale property

In the proof of the pricing PDE in Appendix B, we assume that $g_N(\cdot, \cdot)/M(\cdot)$ is a martingale under the risk-neutral $\mathbb{Q}$-measure. In this section, we numerically confirm that this is case.

The dynamics of $g_N(\cdot, \cdot)/M(\cdot)$ are given by

$$\mathrm{d}\left(\frac{g_N(t, X(t))}{M(t)} \right) = \frac{1}{M(t)} \left(\overline{\mu}^{\mathbb{Q}}(t, X(t)) - r g_N(t, X(t)) \right) \mathrm{d}t + \frac{\partial g_N}{\partial X} \sigma(t, X(t)) \mathrm{d}W^{\mathbb{Q}}(t),$$

with

$$\overline{\mu}^{\mathbb{Q}}(t, X(t)) := \frac{\partial g_N}{\partial t} + \mu^{\mathbb{Q}}(t, X(t)) \frac{\partial g_N}{\partial X} + \frac{1}{2} \frac{\partial^2 g_N}{\partial X^2} \sigma^2(t, X(t)). \tag{2.6}$$

Taking the expectation of its solution under the risk-neutral $\mathbb{Q}$-measure gives

$$\mathbb{E}^{\mathbb{Q}}\left[\frac{g_N(T,X(T))}{M(T)}\right] = \frac{g_N(0,X(0))}{M(0)} + \mathbb{E}^{\mathbb{Q}}\left[\int_0^T \frac{1}{M(t)}\left(\overline{\mu}^{\mathbb{Q}}(t,X(t)) - r g_N(t,X(t))\right)\mathrm{d}t\right] + \mathbb{E}^{\mathbb{Q}}\left[\int_0^T \frac{\partial g_N}{\partial X}\sigma(t,X(t))\mathrm{d}W^{\mathbb{Q}}(t)\right]. \quad (2.7)$$

Trivially, the latter expectation in (2.7) equals 0. In order for $g_N(\cdot,\cdot)/M(\cdot)$ to be a martingale, the former expectation needs to be 0 as well. We numerically confirm this for $X(\cdot)$ being governed by an Ornstein-Uhlenbeck process,

$$\mathrm{d}X(t) = \kappa\left(\theta - X(t)\right)\mathrm{d}t + \gamma \mathrm{d}W^{\mathbb{Q}}(t),\ X(0) = X_0,$$

implying $X(t) \overset{\mathrm{d}}{=} \mathcal{N}(\mu_X(t), \sigma_X^2(t))$, with

$$\mu_X(t) = X_0 \mathrm{e}^{-\kappa t} + \theta\left(1 - \mathrm{e}^{-\kappa t}\right), \quad \sigma_X^2(t) = \frac{\gamma^2}{2\kappa}\left(1 - \mathrm{e}^{-2\kappa t}\right). \quad (2.8)$$

The first expectation in (2.7), assuming $r = 0$, is given by

$$\mathbb{E}\left[\int_0^T \left(\frac{\partial g_N(t,X(t))}{\partial t} + \kappa\left(\theta - X(t)\right)\frac{\partial g_N(t,X(t))}{\partial X} + \frac{1}{2}\gamma^2 \frac{\partial^2 g_N(t,X(t))}{\partial X^2}\right)\mathrm{d}t\right]. \quad (2.9)$$

We choose the kernel parameter values $X_0 = 1,\ \kappa = 0.5,\ \gamma = 0.5$ and $\theta = 0.1$. We assume a Heston market parameterization with $\kappa = 0.5,\ \gamma = 0.5,\ \rho_{x,v} = -0.5,\ V_0 = 0.1$ and $\overline{V} = 0.1$. Further, $T = 5$. We calculate collocation points $x_{i,j} := x_j(T_i)$ and corresponding collocation values $s_{i,j} := s_j(T_i)$ for expiries T_i typically quoted in the FX market[2] and apply Lagrange interpolation:

$$s(t) \approx g_N(t,x) := \sum_{i=1}^N s_i(t)\ell_i(t,x), \quad \ell_i(t,x) := \prod_{j=1,\, j\neq i}^N \frac{x - x_j(t)}{x_i(t) - x_j(t)},$$

with (see also [20])

$$x_j(t) = \mu_X(t) + \sigma_X(t)\cdot z_j,\ j = 1,\ldots,N,$$

where $\mu_X(\cdot)$ and $\sigma_X(\cdot)$ are given in (2.8) and z_j are the collocation points corresponding to $Z \overset{\mathrm{d}}{=} \mathcal{N}(0,1)$. The collocation value $s_j(\cdot)$ is obtained by linear interpolation between the values $s_{i,j}$. For different numbers of collocation points N we compute the absolute value of (2.9), i.e.

$$\epsilon := \left|\int_{-\infty}^{+\infty}\int_0^T \left(\frac{\partial g_N(t,x)}{\partial t} + \kappa\left(\theta - x\right)\frac{\partial g_N(t,x)}{\partial x} + \frac{1}{2}\gamma^2\frac{\partial^2 g_N(t,x)}{\partial x^2}\right) f_{X(t)}(x)\mathrm{d}t\mathrm{d}x\right|. \quad (2.10)$$

Results are displayed in Figure 2.1. An exponential convergence is observed, which is in line with [2].

3 The OU-CLV, CIR-CLV and Heston-CLV models

As already mentioned in [21], the kernel process (2.2) can be specified in principle freely. In the case that its moments are analytically available and numerically stable, the optimal collocation points can be established (see Remark 2.1 and Appendix A) – however, this is not a strict requirement.

The choice of an appropriate kernel process is subtle. On one hand, the process should be evaluated efficiently, e.g. the Monte Carlo simulation may consist of large time-steps.

[2]Namely the expiries 1/365, 2/365, 3/365, 4/365, 1/52, 2/52, 1/12, 1/6, 1/4, 1/2, 3/4, 1, 2, 3, 4 and 5.

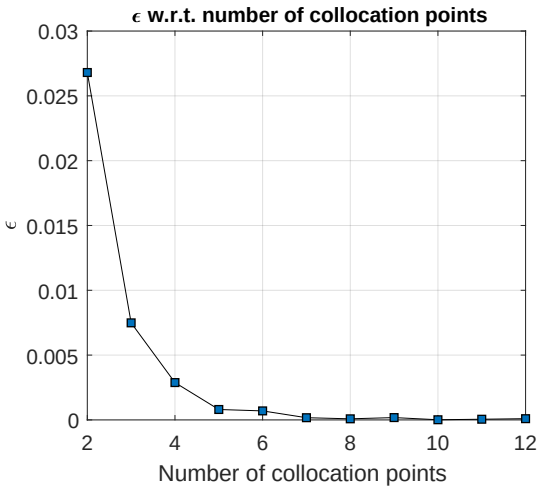

Figure 2.1: The absolute value of the expectation (2.9) for different numbers of collocation points.

On the other hand, the process should be sufficiently rich to represent realistic dynamics, implying a *realistic forward smile behaviour*. According to Clark [9] neither the 'sticky-delta' property of stochastic volatility models nor the 'sticky-strike' characteristic corresponding to the local volatility model is in line with the actual smile behaviour in FX markets; the reality is somewhere between the two and therefore typically a stochastic local volatility model is used.

In this section we discuss three different choices for the kernel process, namely an Ornstein-Uhlenbeck (OU), a Cox-Ingersoll-Ross (CIR) and a Heston process. We discuss the main characteristics of the OU-CLV, CIR-CLV and Heston-CLV models and give special attention to the forward smiles. More specifically, for each of the kernel processes we consider the effect of the various kernel parameters on the shape of the forward smile. Based on this analysis, we calibrate the OU-CLV, CIR-CLV and Heston-CLV models to FX barrier options in Section 4.

3.1 The OU-CLV model

The OU-CLV model is given by the following equations, under the risk-neutral $\mathbb{Q}$-measure:

$$S(t) = g_N(t, X(t)), \tag{3.1}$$

$$\mathrm{d}X(t) = \kappa\left(\theta - X(t)\right)\mathrm{d}t + \gamma \mathrm{d}W^{\mathbb{Q}}(t),\ X(t_0) = X_0. \tag{3.2}$$

Remark 3.1 (Specification of $X(\cdot)$)**.** *Given the filtration at $t_0 = 0$, the solution to (3.2) reads*

$$X(t) = X_0 \mathrm{e}^{-\kappa t} + \theta\left(1 - \mathrm{e}^{-\kappa t}\right) + \frac{\gamma}{\sqrt{2\kappa}} \mathrm{e}^{-\kappa t} W^{\mathbb{Q}}\left(\mathrm{e}^{2\kappa t} - 1\right), \tag{3.3}$$

which is normally distributed with the mean and variance as in (2.8).

As the moments of $X(\cdot)$ are analytically available and numerically stable, we can calculate the optimal collocation points [20, 21] resulting in exponential convergence with respect to the number of collocation points. Also, as the distribution of $X(\cdot)$ is known, for the pricing of a standard European-type option by the OU-CLV model *one* time-step is sufficient; in step 3 of Algorithm 1, $X(T)$ is generated by sampling $\mathcal{M}$ realizations $x_m,\ m = 1, \ldots, \mathcal{M}$ from a normal random variable with mean and variance as in equation (2.8).

For the pricing of exotics though, multiple time-steps are necessary, see e.g. the numerical experiment in Appendix C where we price a discretely monitored barrier option. Whether this price is realistic, depends on the *forward smile* the OU-CLV model implies. We therefore

consider the smile corresponding to a *forward-start option*, which provides the holder at a future time $T_1 > t_0$ with a European option with a maturity $T_2 > T_1$ and a strike $K \cdot S(T_1)$. At T_2 the pay-off of this option of the 'call type' is [29]:

$$V_{\text{Forw.St.}} = \max\left(S(T_2) - K \cdot S(T_1), 0\right). \tag{3.4}$$

Numerical experiments make clear that only the mean reversion parameter κ has an effect on the forward smile corresponding to the OU-CLV model – see Figure[3] 3.1. On the right-hand side we display the forward volatility smiles omitting the level effect to make the curvature effect visible (more precisely, we shift the smile downwards such that its minimum is at 0). The primary effect of the mean reversion parameter is on the level: an increase in κ yields an increase in level. A secondary effect is on the curvature, see the right-hand plot of Figure 3.1. As mentioned in [21], changing κ affects the filtration of the Brownian motion of the solution of $X(\cdot)$ in (3.3). As such, an OU process with mean reversion parameter κ_1 cannot be expressed as a linear combination of an OU process with a different mean reversion parameter value κ_2. Because of this, a change of κ affects the autocorrelation of the paths of $g_N(\cdot,\cdot)$ and the forward smile. In Table 1 we summarize the kernel parameter effects on the shape of the forward smile.

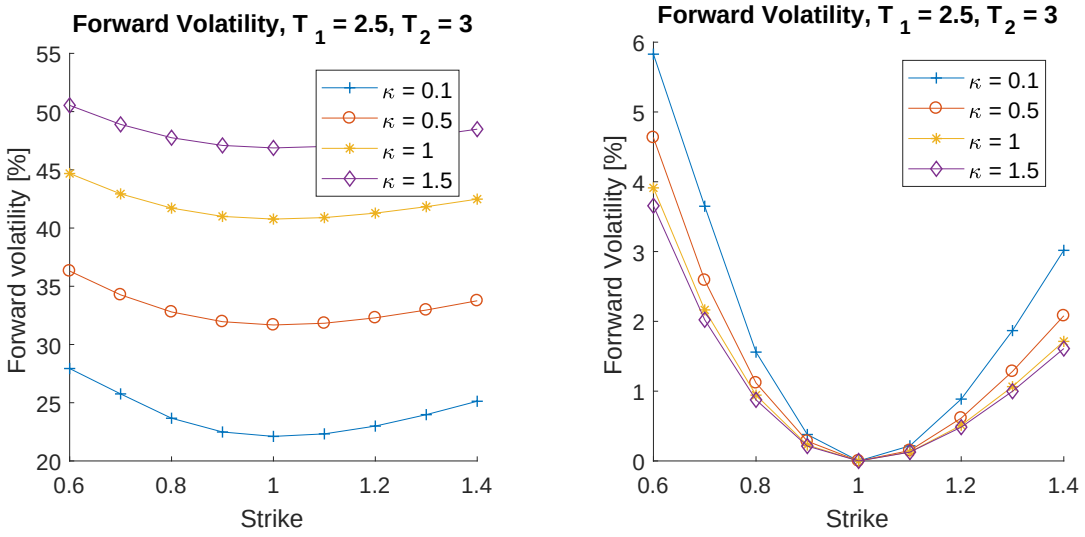

Figure 3.1: Effect of κ on the forward volatility smile for the OU-CLV model, with $T_1 = 2.5$ and $T_2 = 3$. In the right-hand plot all smiles are shifted to zero level to make the curvature effect more visible. Other OU parameters are: $X_0 = 1$, $\gamma = 0.3$, $\theta = 0.5$.

	Level	**Curvature**	**Skewness**
κ	+	-	0
γ	0	0	0
X_0	0	0	0
θ	0	0	0

Table 1: Separate effects of the OU kernel parameters on the level, curvature and skewness of the forward smile implied by the OU-CLV model. A '+'/'-' represents a higher/lower volatility smile level, more/less curvature or more/less skewness in the case of increasing a particular kernel parameter. A '0' stands for no effect.

[3] We omit the pictures corresponding to the other kernel parameters, as no effect was observed. We assume a Heston market parameterization with parameters $\kappa = 0.5$, $\gamma = 0.3$, $\rho_{x,v} = -0.1$, $v_0 = 0.04$ and $\overline{v} = 0.04$. Also, $r = 0$ and $S_0 = 1$. Further, we use $N = 6$ collocation points and 2 time-steps per year and $5 \cdot 10^5$ paths in the Monte Carlo simulation (5 seeds, each seed constitutes $1 \cdot 10^5$ paths).

3.2 The CIR-CLV model

The Cox Ingersoll Ross-Collocating Local Volatility (CIR-CLV) model is represented by the following two equations, under the risk-neutral $\mathbb{Q}$-measure:

$$\begin{aligned} S(t) &= g_N(t, X(t)), & (3.5)\\ \mathrm{d}X(t) &= \kappa\left(\theta - X(t)\right)\mathrm{d}t + \gamma\sqrt{X(t)}\mathrm{d}W^{\mathbb{Q}}(t),\ X(t_0) = X_0. & (3.6)\end{aligned}$$

Result 3.1 (Specification of $X(\cdot)$)**.** *Given the filtration at $t_0 = 0$, the solution to (3.6) is distributed as a scaled non-central chi-square random variable $\chi^2(d, \lambda(t))$ with d degrees of freedom and non-centrality parameter $\lambda(t)$, i.e.*

$$X(t) \overset{\mathrm{d}}{=} c(t)\Lambda(t),\ \textit{with}\ \Lambda(t) \overset{\mathrm{d}}{=} \chi^2(d, \lambda(t)), \tag{3.7}$$

where

$$c(t) = \frac{1}{4\kappa}\gamma^2\left(1 - \mathrm{e}^{-\kappa t}\right),\ d = \frac{4\kappa\theta}{\gamma^2},\ \lambda(t) = \frac{4\kappa X_0 \mathrm{e}^{-\kappa t}}{\gamma^2(1 - \mathrm{e}^{-\kappa t})}. \tag{3.8}$$

The nth moment of $\Lambda(t)$ is given by

$$\mathbb{E}\left[\Lambda^n(t)\right] = 2^{n-1}(n-1)!(d + n\lambda(t)) + \sum_{k=1}^{n-1}\frac{(n-1)!2^{k-1}}{(n-k)!}(d + k\lambda(t))\mathbb{E}\left[\Lambda^{n-k}(t)\right].$$

In computing the first moment, the summation term disappears and $0! = 1$, resulting in $\mathbb{E}\left[\Lambda(t)\right] = d + \lambda(t)$, thus

$$\mathbb{E}\left[X(t)\right] = c(t)\left(d + \lambda(t)\right).$$

Generally speaking, we wish to evaluate $x_j(\cdot)$ based on the moments of $X(\cdot)$. This ensures that the collocation points are the zeros of the orthogonal polynomial corresponding to the distribution of $X(\cdot)$, and we can establish the connection with the computation of integrals by Gauss quadrature, see Remark 2.1 and Appendix A. However, for $X(\cdot)$ given by (3.7) an explosion of moments may occur. E.g., for the kernel parameters $X_0 = 1$, $\theta = 1$, $\kappa = 1$, $\gamma = 0.1$ we have at $t = 1$ the values $d = 400,\ \lambda(1) \approx 233$. Given these values, the 4th moment of $\Lambda(\cdot) \overset{\mathrm{d}}{=} \chi^2(d, \lambda(t))$ has a value with an order of magnitude of 10^{11}. Due to the large moment values, numerical instabilities in computing the collocation points may occur[4]. As an alternative approach, we use the collocation points $z_j,\ j = 1, \ldots, N$ corresponding to the standard normal random variable $Z \overset{\mathrm{d}}{=} \mathcal{N}(0, 1)$ – see Remark 3.2. Given these, we compute the collocation points corresponding to expiry $T_i,\ i = 1, \ldots, M$, as follows:

$$x_{i,j} := x_j(T_i) = F^{-1}_{X(T_i)}(F_Z(z_j)) = c(T_i)F^{-1}_{\Lambda(T_i)}(F_Z(z_j)),\ i = 1, \ldots, M,\ j = 1, \ldots, N.$$

Note that this implies the collocation values

$$s_{i,j} = F^{-1}_{S(T_i)}\left(F_{X(T_i)}(x_{i,j})\right) = F^{-1}_{S(T_i)}\left(F_{X(T_i)}(F^{-1}_{X(T_i)}(F_Z(z_j)))\right) = F^{-1}_{S(T_i)}\left(F_Z(z_j)\right), \tag{3.9}$$

which shows that we do *not* need the CDF of $X(\cdot)$ for computing the collocation values.

Remark 3.2 (Normal distribution)**.** *The reason why we choose a standard normal distribution in the alternative approach is twofold. First, even for a fundamental distribution as the standard normal results are highly accurate – this is also the case in e.g. [20, 21]. By choosing a different distribution, results may be further enhanced. Secondly, as mentioned in [20], choosing the normal distribution is also motivated by the Cameron-Martin Theorem [7], which states that polynomial chaos approximations based on the normal distribution converge to any distribution.*

[4]For example, for $N = 8$ we obtain negative collocation points, although the distribution of $X(\cdot)$ does not allow for negative values.

Remark 3.3 (Loss of optimality of collocation points)**.** *A drawback of the alternative approach is that the collocation points are not the zeros of the orthogonal polynomial $p_N(\cdot)$ that corresponds to the weight function $f_X(\cdot)$, with X denoting the non-central chi-square distributed random variable – see also Appendix A. As a consequence, the method can not be connected to Gauss quadrature, see equations (A.1) and (A.2) in Appendix A, as the x_i-values do not correspond to the quadrature weights ω_i, which are one-to-one connected to the weight function $f_X(\cdot)$. In fact, there would be a mismatch between the x_i and ω_i values and the error is not longer (completely) determined by the quadrature error.*

Remark 3.4 (The case $\gamma = 0$)**.** *In the case $\gamma = 0$, the OU and CIR kernel processes (3.2) and (3.6) are equivalent and deterministic. This is not a relevant case, as the CLV framework relies on the projection of an 'expensive' random variable on a 'cheaper' random variable, which is the essence of stochastic collocation.*

3.2.1 Effect of 'linearization'

As we stated in Remark 2.2, optimal results are established if for a given t the distributions of $X(t)$ and $S(t)$ approximately resemble each other. For an expiry T_i this implies a close-to-linear relation between the collocation points $x_{i,j}$ and collocation values $s_{i,j}$, through which $g_N(\cdot,\cdot)$ interpolates. Given a set of market data and a set of kernel parameters, it may turn out though that $g_N(\cdot,\cdot)$ is highly non-linear, which may affect the performance of the stochastic collocation method and the eventual fit of the CLV model to European-type market prices negatively.

For illustration purposes, suppose that the market data is parameterized by the Heston model, with parameters given by Case II of Andersen [1]: $v_0 = \overline{v} = 0.04$, $\kappa = 0.3$, $\gamma = 0.9$ and $\rho_{xv} = -0.5$. Also, $r = 0$ and $S_0 = 1$. We choose kernel parameters[5] $\gamma = 1.5$, $\kappa = 0.5$, $\theta = 0.5$, $X_0 = 1$, and price a European call option with expiry $T = 4$; results are displayed in Figure 3.2. To judge the performance of the interpolant $g_N(t,x)$, we display the theoretical function

$$g(t,x) := F^{-1}_{Y(t)}\left(F_{X(t)}(x)\right) = F^{-1}_{S(t)}\left(F_{\Lambda(t)}\left(\frac{x-a(t)}{c(t)b(t)}\right)\right),$$

with $a(\cdot)$ and $b(\cdot)$ denoting grid-stretching coefficients [20] and $Y(t) = S(t)$ representing the 'expensive' random variable which we project on the kernel variable $X(t) \overset{\mathrm{d}}{=} c(t)\Lambda(t)$ with $\Lambda(t) \overset{\mathrm{d}}{=} \chi^2(d,\lambda(t))$ ($c(t)$ and $\lambda(t)$ are specified in (3.8)).

As we observe in the middle plot of Figure 3.2, the CDF of $g_N(\cdot,\cdot)$ is clearly not in line with the market-implied CDF. As a result, the implied volatility fit for the lower 2 strikes is not accurate. The reason for this lies in the highly non-linear behaviour of $g_N(\cdot,\cdot)$ close to zero. A way to resolve this issue is by adjusting the kernel parameters such that the relation between $S(\cdot)$ and $X(\cdot)$ is closer to linear. Setting $\gamma = 0.75$ results in a better performance of the CLV method close to $x = 0$ and implies a more accurate implied volatility fit, see Figure 3.3.

3.2.2 The forward smile

In this section we consider the effect of the CIR kernel parameters on the forward smile corresponding to the CIR-CLV model by pricing a forward-start option, with a pay-off at T_2 given by (3.4). *With a 'positive effect' we mean that increasing a particular kernel parameter results in a higher volatility smile level, more curvature or skewness.* Results[6] are given in

[5] We use 8 collocation points and make use of grid-stretching with $p_{\min} = 1 \cdot 10^{-3}$ and $p_{\max} = 0.999$ – for more details on grid-stretching, see e.g. [20]. The Monte Carlo simulation constitutes $1 \cdot 10^5$ paths (20 seeds, each seed constitutes $5 \cdot 10^3$ paths) and 1 time-step per year.

[6] We assume a Heston market parameterization with parameters $\kappa = 0.5$, $\gamma = 0.3$, $\rho_{x,v} = -0.1$, $v_0 = 0.04$ and $\overline{v} = 0.04$. Also, $r = 0$ and $S_0 = 1$. Further, we use $N = 8$ collocation points, apply grid-stretching with $p_{\min} = 1 \cdot 10^{-3}$ and $p_{\max} = 0.999$ and the Monte Carlo simulation consists of 2 time-steps per year and $5 \cdot 10^5$

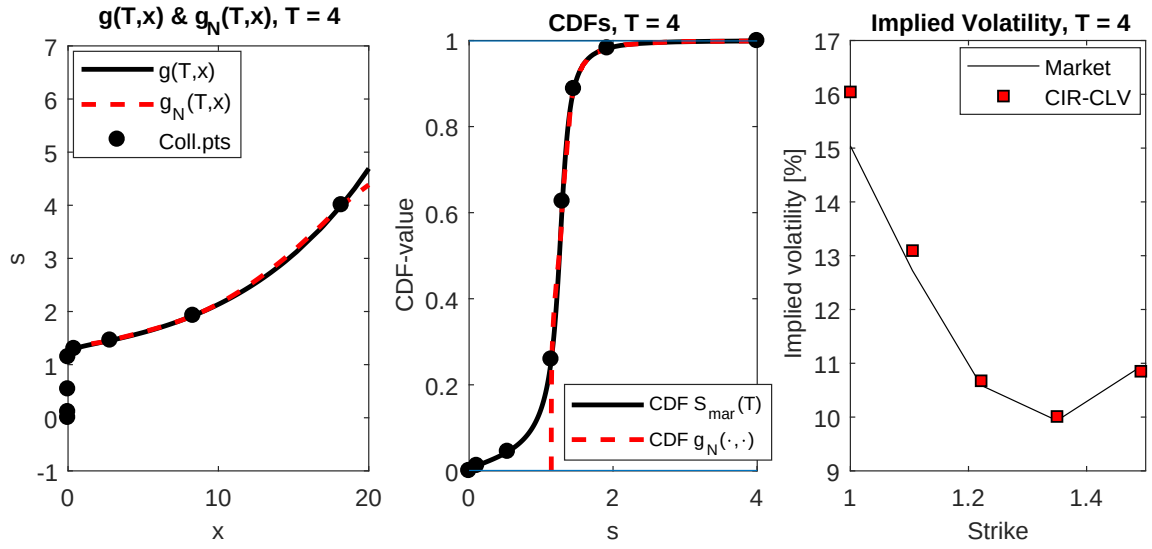

Figure 3.2: Results for the case described in Section 3.2.1, with $\gamma = 1.5$. With 'CDF $S_{\text{mar}}(T)$' we denote the market-implied CDF specified in equation (2.3).

Figures 3.4 and 3.5. We clearly observe that the volatility of variance has a positive effect on both the level and the curvature of the forward smile. The speed of mean reversion has mainly a positive level effect, but also a negative curvature effect, i.e. a larger value of κ implies *less* curvature. Further, X_0 only has a negative level effect. Last, θ has a positive level effect and a slightly negative curvature effect.

Some effects may be quite difficult to observe due to the level effect. As such, in Appendix D we display Figures 3.4 and 3.5, but without the level effect. In Table 2 we summarize the effects of the CIR parameters on the forward smile.

	Level	**Curvature**	**Skewness**
γ	+	+	0
κ	+	−	0
X_0	−	0	0
θ	+	−	0

Table 2: Separate effects of the CIR kernel parameters on the level, curvature and skewness of the forward smile implied by the CIR-CLV model. A '+'/'-' represents a higher/lower volatility smile level, more/less curvature or more/less skewness in the case of increasing a particular kernel parameter. A '0' stands for no effect.

3.3 The Heston-CLV model

The Heston-CLV model is defined as follows:

$$\begin{aligned} S(t) &= g_N(t, X(t)), \\ \mathrm{d}X(t) &= rX(t)\mathrm{d}t + \sqrt{v(t)}X(t)\mathrm{d}W_x(t),\ X(0) = X_0, \\ \mathrm{d}v(t) &= \kappa\left(\overline{v} - v(t)\right)\mathrm{d}t + \gamma\sqrt{v(t)}\mathrm{d}W_v(t),\ v(0) = v_0, \end{aligned}$$

with $\mathrm{d}W_x(t)\mathrm{d}W_v(t) = \rho_{x,v}\mathrm{d}t$ and where κ, γ, $\overline{v}$ and $\rho_{x,v}$ are the rate of mean reversion, the volatility of variance, the long-term variance and the correlation, respectively. According to [25], the Heston model stands out from the class of stochastic volatility models mainly for two reasons. First, the volatility process is non-negative and mean-reverting, which is typically

paths (5 seeds, each seed constitutes $1 \cdot 10^5$ paths).

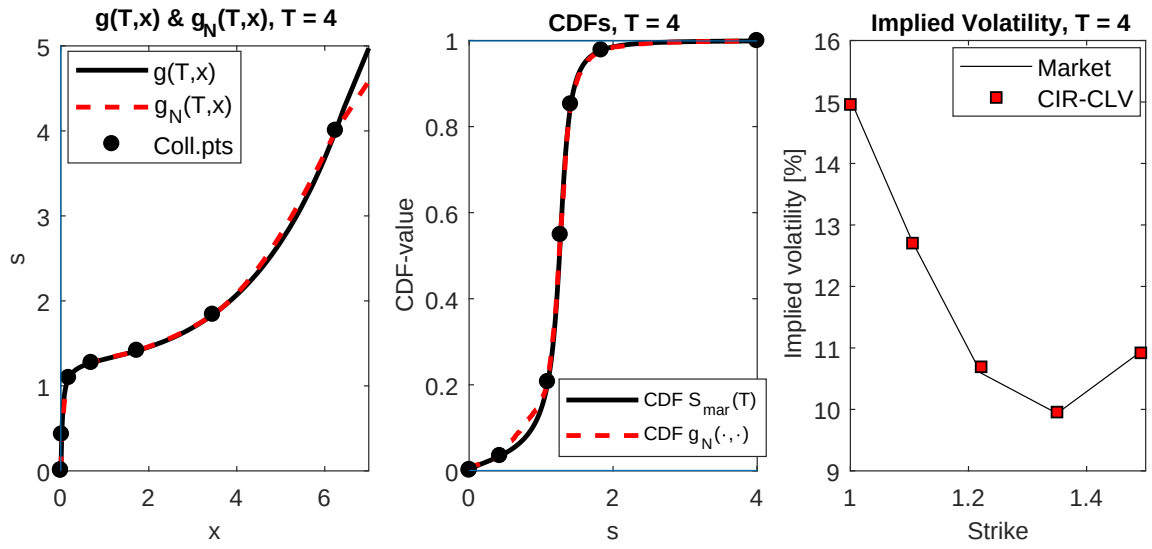

Figure 3.3: Results for the case described in Section 3.2.1, with $\gamma = 0.75$. With 'CDF $S_{mar}(T)$' we denote the market-implied CDF specified in equation (2.3).

observed in the markets. Secondly, a fast and easily implemented semi-analytical solution for the pricing of European-type options is available. In particular, efficient numerical Fourier-based techniques exist, which allow for a fast calibration.

3.3.1 Establishing $x_{i,j}$ and $s_{i,j}$

From the characteristic function of $\widehat{X}(\cdot) := \log(X(\cdot))$ (see e.g. [13]), which is defined as

$$\phi_{\widehat{X}(t)}(u) := \mathbb{E}\left[\mathrm{e}^{iu\widehat{X}(t)}\middle|\mathcal{F}(t_0)\right],$$

we may compute the kth moment of $X(t)$ as follows (we suppress the condition on $\mathcal{F}(t_0)$ for notation purposes):

$$\phi_{\widehat{X}(t)}(-ki) = \mathbb{E}\left[\mathrm{e}^{k\widehat{X}(t)}\right] = \mathbb{E}\left[\mathrm{e}^{k\log(X(t))}\right] = \mathbb{E}\left[X^k(t)\right].$$

From the moments of $X(\cdot)$ we obtain the collocation points $x_{i,j}, i = 1, 2, \ldots, M, j = 1, 2, \ldots, N$.

There is a drawback to this approach though. One element of the characteristic function of the Heston model is $\sqrt{(\kappa - \gamma\rho_{x,v}iu)^2 + (u^2 + iu)\gamma^2}$. When an *imaginary argument* u is used, it cannot be guaranteed that the expression below the square root is non-negative, which may result in inaccurate numerical moment values.

As an alternative approach, similar to the CIR-CLV model, we use the collocation points $z_j,\ j = 1, \ldots, N$ corresponding to the standard normal random variable $Z \overset{\mathrm{d}}{=} \mathcal{N}(0,1)$ – see also Remark 3.2. Given these, we compute the collocation points corresponding to expiry $T_i,\ i = 1, \ldots, M$, according to

$$x_{i,j} := x_j(T_i) = F^{-1}_{X(T_i)}(F_Z(z_j)), \tag{3.10}$$

and the collocation values as in (3.9).

To compute the collocation points according to (3.10), we define $\widehat{X}(\cdot) := \log(X(\cdot))$ and note

$$F_{X(T_i)}(x_{i,j}) = F_{\widehat{X}(T_i)}(\widehat{x}_{i,j}).$$

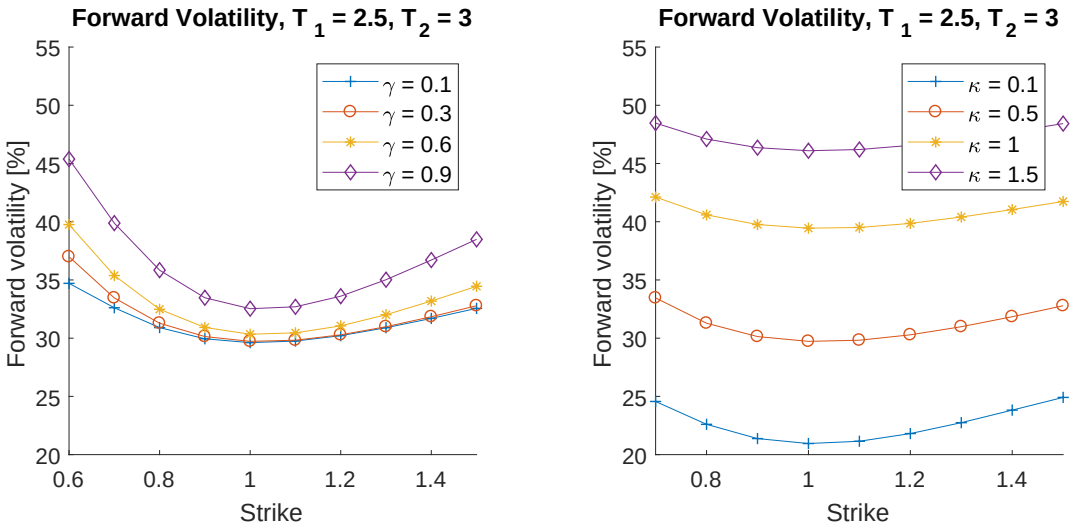

Figure 3.4: Effect of γ (left) and κ (right) on the forward volatility smile for the CIR-CLV model, with $T_1 = 2.5$ and $T_2 = 3$. The 'base case' CIR parameters (if not varied) are: $\gamma = 0.3$, $\kappa = 0.5$, $\theta = 0.5$ and $X_0 = 1$.

The CDF of $\widehat{X}(\cdot)$ can be obtained efficiently in a 'COS-like' fashion, see [13]. Given the approximation for its PDF[7]

$$f_{\widehat{X}(t)}(x) \approx {\sum_{k=0}^{N-1}}' F_k \cos\left(k\pi \frac{x-a}{b-a}\right), \quad F_k = \frac{2}{b-a}\mathrm{Re}\left\{\phi_{\widehat{X}(t)}\left(\frac{k\pi}{b-a}\right)\cdot \exp\left(-i\frac{ka\pi}{b-a}\right)\right\},$$

with N denoting the number of terms[8], we obtain the CDF of $\widehat{X}(\cdot)$ as follows:

$$F_{\widehat{X}(t)}(x) = {\sum_{k=0}^{N-1}}' \frac{2}{b-a}\mathrm{Re}\left\{\phi_{\widehat{X}(t)}\left(\frac{k\pi}{b-a}\right)\cdot \exp\left(-i\frac{ka\pi}{b-a}\right)\right\}\psi_k(a,b,x),$$

with

$$\psi(a,b,x) = \begin{cases} \frac{b-a}{k\pi}\sin\left(k\pi\frac{x-a}{b-a}\right), & \text{if } k = 1,2,\ldots,N-1, \\ x-a, & \text{if } k = 0. \end{cases}$$

Given the CDF, we obtain $\widehat{x}_{i,j} = F^{-1}_{\widehat{X}(T_i)}(F_Z(z_j))$ and $x_{i,j} = \mathrm{e}^{\widehat{x}_{i,j}}$.

3.3.2 Choice of X_0 and r

An initial calibration of the Heston kernel parameters may enhance the performance of the CLV model, in particular of the stochastic collocation method, as a pre-calibration may 'linearize' the relationship between $S(\cdot)$ and the kernel parameter $X(\cdot)$ – see Remark 2.2 and Section 3.2.1. Essentially, this means that we prefer that $X(\cdot)$ and $S(\cdot)$ are similar in a distributional sense, which yields a small approximation error [20] and a more optimal performance of the stochastic collocation method.

A first 'calibration' step is by determining values for certain kernel process parameters such that the following condition holds ('first moment matching'):

$$\mathbb{E}^{\mathbb{Q}}[X(t)] = F(0,t), \text{ for all } t \in [0,T], \tag{3.11}$$

[7]Note that ${\sum}'_{k=0}^{N-1}$ represents a summation where the first term ($k = 0$) is multiplied by $1/2$.
[8]In our numerical experiments we typically use $N = 2^{12}$, $a = -10$ and $b = 10$.

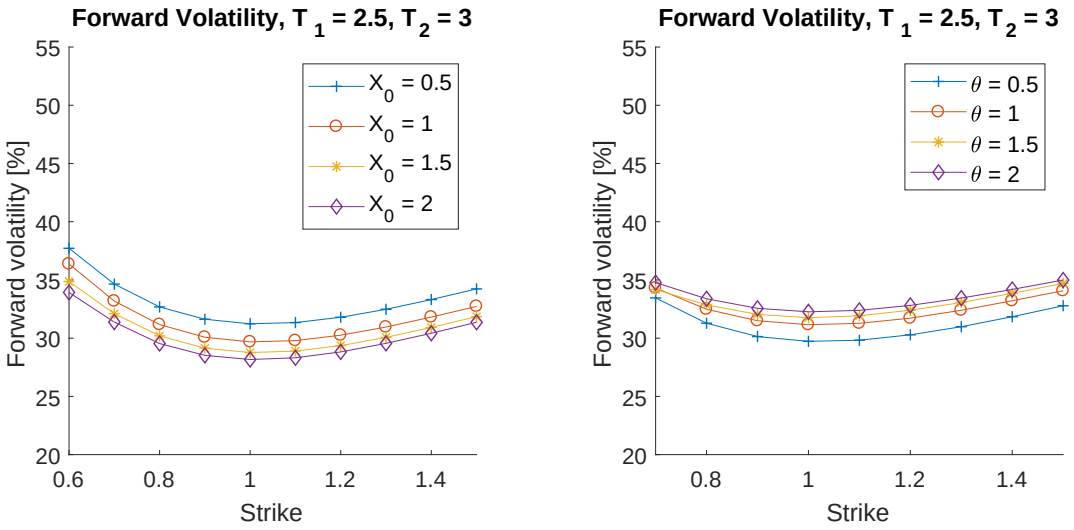

Figure 3.5: Effect of X_0 (left) and θ (right) on the forward volatility smile for the CIR-CLV model, with $T_1 = 2.5$ and $T_2 = 3$. The 'base case' CIR parameters (if not varied) are: $\gamma = 0.3$, $\kappa = 0.5$, $\theta = 0.5$ and $X_0 = 1$.

where the initial forward (in an FX context) is given by

$$F(0,t) = S_0 \frac{P_f(0,t)}{P_d(0,t)} = S_0 \mathrm{e}^{(r_d - r_f)t},$$

with $P_f(0,t)$ and $P_d(0,t)$ denoting the foreign and domestic zero-coupon bond prices, respectively, extracted from the market quotes. For the Heston kernel process (assuming constant interest rate r) a standard result is

$$\mathbb{E}^{\mathbb{Q}}\left[\frac{X(t)}{M(t)}\right] = \mathbb{E}^{\mathbb{Q}}\left[\frac{X(t)}{M_0 \mathrm{e}^{rt}}\right] = \frac{X_0}{M_0}.$$

Assuming $M_0 = 1$ without loss of generality, the previous equation implies

$$\mathbb{E}^{\mathbb{Q}}\left[X(t)\right] = X_0 M(t) = X_0 \mathrm{e}^{rt}. \tag{3.12}$$

From the result in (3.12) we easily see that the condition in (3.11) is satisfied by the kernel process parameter choices $X_0 = S_0$, $r = r_d - r_f$, for *arbitrary* time t and *arbitrary* values of the other kernel parameters κ, γ, $\overline{v}$ and v_0.

3.3.3 The forward smile

In this section we consider the effect of the Heston kernel parameters on the forward smile corresponding to the Heston-CLV model by pricing a forward-start option, with a pay-off at T_2 given by (3.4). We use the Quadratic Exponential (QE) scheme of Andersen [1]. Results[9] are given in Figures 3.6, 3.7 and 3.8.

Increasing γ yields a more pronounced implied volatility smile; the curvature increases. For the parameter κ this effect is opposite; a higher value of κ implies less curvature. The correlation parameter $\rho_{x,v}$ yields a rotation of the smile; varying the parameter from -1 to $+1$ yields a counterclockwise rotation, i.e. less skewness. Besides for that, $\rho_{x,v}$ also has some positive level effect. Further, the long-run variance $\overline{v}$ and the initial variance v_0 mainly have a level effect – note that a larger value of v_0 yields a lower level. X_0 does not have

[9] We assume a Heston market parameterization with parameters $\kappa = 0.5$, $\gamma = 0.3$, $\rho_{x,v} = -0.1$, $v_0 = 0.04$ and $\overline{v} = 0.04$. Also, $r = 0$ and $S_0 = 1$. Further, we use $N = 6$ collocation points and the Monte Carlo simulation consists of 32 time-steps per year and $5 \cdot 10^5$ paths (5 seeds, each seed constitutes $1 \cdot 10^5$ paths).

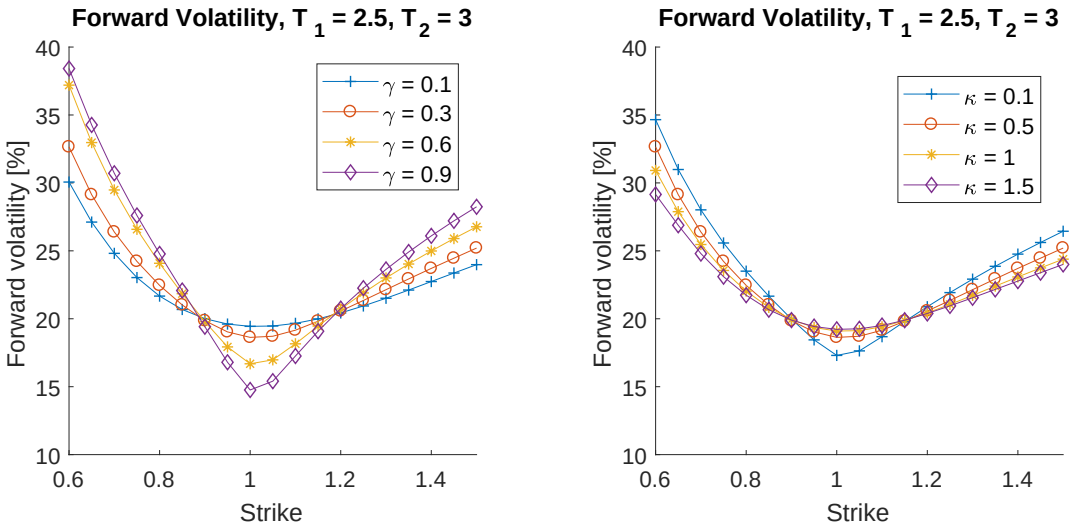

Figure 3.6: Effect of γ (left) and κ (right) on the forward volatility smile for the Heston-CLV model, with $T_1 = 2.5$ and $T_2 = 3$. The 'base case' Heston parameters (if not varied) are: $\kappa = 0.5,\ \gamma = 0.3,\ \rho_{x,v} = 0,\ \overline{v} = 0.2,\ v_0 = 0.2$ and $X_0 = 1$.

	Level	**Curvature**	**Skewness**
γ	0	+	0
κ	0	–	0
$\rho_{x,v}$	+	0	–
$\overline{v}$	+	–	+
v_0	–	0	0
X_0	0	0	0

Table 3: Separate effects of the Heston kernel parameters on the level, curvature and skewness of the forward smile. A '+'/'-' represents a higher/lower volatility smile level, more/less curvature or more/less skewness in the case of increasing a particular kernel parameter. More skewness represents a more *negative* slope of the forward smile, i.e. a *clockwise* rotation. A '0' stands for no effect.

any effect, which implies that a parallel shift of the kernel variable distribution is 'ignored' by the mapping between the distribution of the kernel variable X and the market-implied distribution. We summarize the effect of the kernel parameters on the shape of the forward smile in Table 3. To observe the curvature and skewness effects more clearly, in Appendix E we display Figures 3.6, 3.7 and 3.8 without the level effect.

The effects of the Heston kernel parameters *in the Heston-CLV model* can be compared to the effects of the parameters in the standard Heston model – see e.g. [38]. In both the Heston-CLV model and the Heston model the volatility of variance γ (mainly) has a positive effect on the curvature of the smile[10]. For both models the initial variance v_0 and the long-term variance $\overline{v}$ have a level effect, although for the Heston-CLV model v_0 has a negative effect on the level, whereas in the Heston model this is positive. In both the Heston-CLV model and the Heston model the mean reversion parameter κ has a negative curvature effect. In both models the correlation parameter $\rho_{x,v}$ (mainly) accounts for the skewness ('steepness') of the smile – in both models a more negative correlation implies a more negative slope, i.e. more skewness. For the Heston-CLV model though $\rho_{x,v}$ also has some level effect.

[10] In this short paragraph on the qualitative effects of the Heston model parameters we make use of [38], which merely mentions the first-order effects. It *may* be possible that the parameters have second-order effects, which is the case for e.g. the Heston-Displaced Diffusion model, see [32].

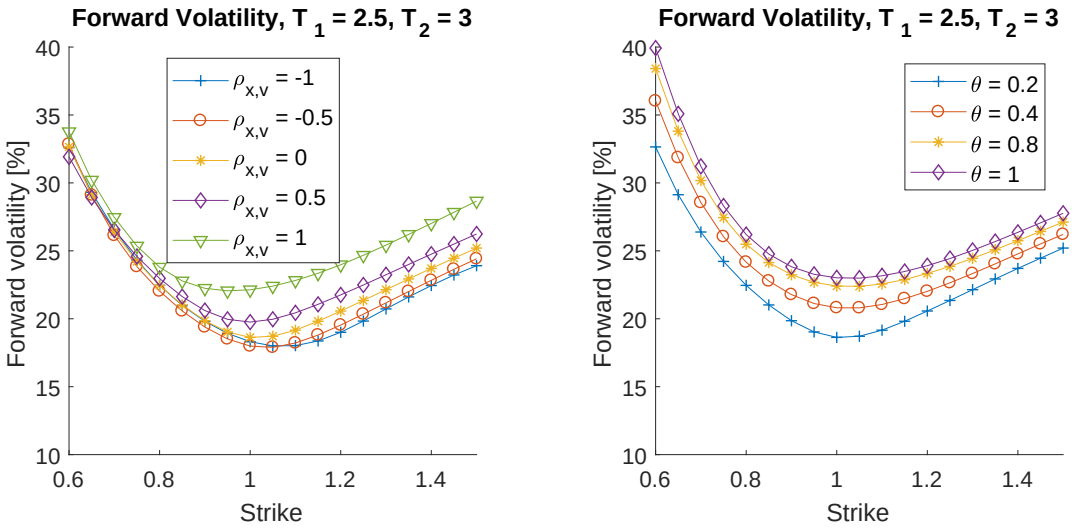

Figure 3.7: Effect of $\rho_{x,v}$ (left) and $\overline{v}$ (right, denoted by θ) on the forward volatility smile for the Heston-CLV model, with $T_1 = 2.5$ and $T_2 = 3$. The 'base case' Heston parameters (if not varied) are: $\kappa = 0.5$, $\gamma = 0.3$, $\rho_{x,v} = 0$, $\overline{v} = 0.2$, $v_0 = 0.2$ and $X_0 = 1$.

4 Calibration to FX barrier options

The CLV model, by its flexibility in controlling the forward smile and its rapid Monte Carlo evaluation, allows for an efficient Monte Carlo calibration to exotic options, while the fit to European-type options is preserved. In this section we calibrate the OU-CLV, CIR-CLV and Heston-CLV models to FX barrier options by Monte Carlo simulation.

The transition densities between future states are reflected by the forward smile a model implies. As a consequence, in the calibration of the CLV model to barrier options we should calibrate the kernel parameters which affect the forward smile. Moreover, ideally, given particular kernel dynamics, to achieve the most accurate calibration we should calibrate kernel parameters which affect *different characteristics* of the shape of the forward smile, namely its level, curvature and skewness.

If the distribution of the kernel variable is analytically known, one time-step is sufficient to price back European-type options – this e.g. holds for the OU-CLV and CIR-CLV models. In the case of a discretely monitored barrier option, for these models the kernel process only needs to be simulated on a time grid consisting of the monitoring dates, see e.g. the numerical example in Appendix C.

In the case of a continuously monitored barrier option, the kernel process needs to be simulated on a dense time-grid – the barrier option is typically monitored on a daily basis, which implies 250 time-steps (business days) per year. To accelerate the Monte Carlo calibration procedure of the kernel parameters to continuously monitored barrier options, we employ *Brownian bridge* techniques, which we describe in Section 4.2. First however, in Section 4.1 we describe the general steps of applying the CLV model in a Monte Carlo simulation framework.

4.1 Monte Carlo simulation framework

In this article we apply the CLV model in a Monte Carlo simulation framework. Its evaluation basically consists of three parts. First, we compute the collocation points and collocation values. Subsequently, we simulate the kernel variable and compute the local volatility function for the time-points of interest. Last, given the local volatility function values, we establish the price of the relevant financial contract in a standard way. In Algorithm 1 we describe the steps in more detail. Note that in the calibration to exotics we repeatedly perform steps **2**, **3** and **4** for different kernel parameter value 'candidates'. In Appendix C we present a basic

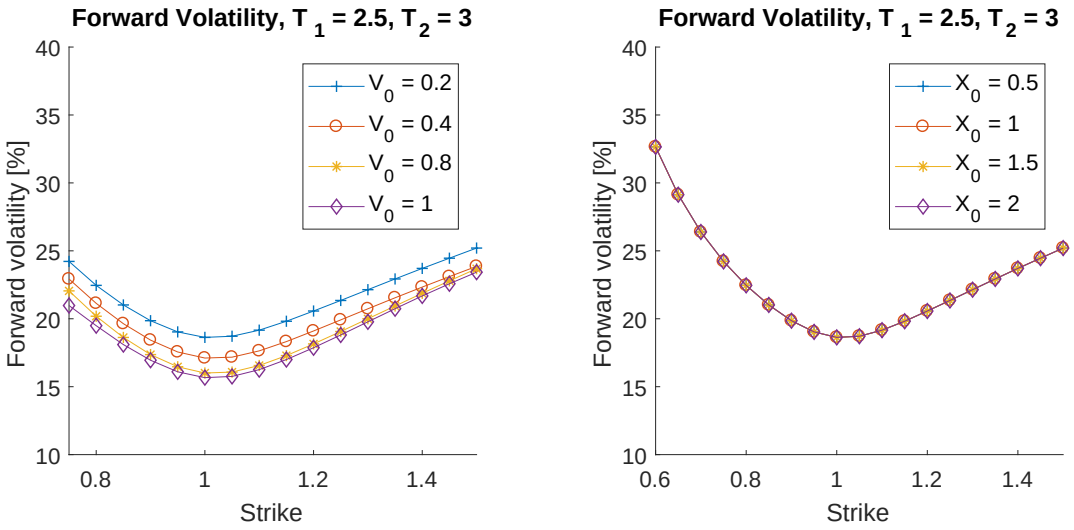

Figure 3.8: Effect of v_0 (left) and X_0 (right) on the forward volatility smile for the Heston-CLV model, with $T_1 = 2.5$ and $T_2 = 3$. The 'base case' Heston parameters (if not varied) are: $\kappa = 0.5,\ \gamma = 0.3,\ \rho_{x,v} = 0,\ \overline{v} = 0.2,\ v_0 = 0.2$ and $X_0 = 1$.

1 Given liquid European-type option prices $V(T_i, K_\ell)$, $i = 1, \ldots, M,\ \ell = 1, \ldots, L$, establish for each expiry T_i the market-implied CDF $F_{S(T_i)}(x)$ as given in equation (2.3), which may be in a parameterized form.

2 For each expiry T_i compute N collocation points $x_{i,1}, \ldots, x_{i,N}$ and the corresponding collocation values $s_{i,1}, \ldots, s_{i,N}$ via $s_{i,j} = F^{-1}_{S(T_i)}(F_{X(T_i)}(x_{i,j}))$, $j = 1, \ldots, N$.

3 Simulate the kernel variable $X(\cdot)$. At relevant time-points t_k, $k = 1, \ldots, K$ in the simulation, compute $g_N(t_k, x_{k,m})$, with $x_{k,m}$ denoting the value of $X(t_k)$ corresponding to the mth path, $m = 1, \ldots, \mathcal{M}$.

4 Compute the price of the relevant financial contract.

Algorithm 1: Applying the CLV model in a Monte Carlo simulation framework.

numerical experiment in which we perform the steps in Algorithm 1 to price a discretely monitored barrier option.

Remark 4.1 (Evaluation of the market-implied CDF)**.** *Regarding the market-implied CDF in step 1 in Algorithm 1, the derivative in (2.3) may be computed by finite differences. However, this approach may not be arbitrage-free as inter- and extrapolation of market volatilities or prices needs to be applied. Another possibility is first calibrating a particular parameterization to the market quotes, enabling us to compute the derivative in (2.3) (semi-)analytically, by e.g. an arbitrage-free 'Hagan implied density' [22] or Fourier-based pricing techniques, see e.g. [8].*

Figure 4.1 provides an illustration of the CLV model in a Monte Carlo simulation framework. The local volatility function $g_N(\cdot, \cdot)$ transforms the original paths of the kernel variable in such a way that the resulting $S(\cdot)$-paths yield a perfect calibration to liquid market quotes.

4.2 Pricing barrier options: a Brownian bridge approach

Pricing continuously monitored barrier options by a Monte Carlo simulation implies an approximation, as we make steps in time and as such monitor on a discrete basis. A way to reduce the error introduced by this approximation is by making use of Brownian bridge techniques [4, 18, 19], where the *conditional hitting probability* is taken into account.

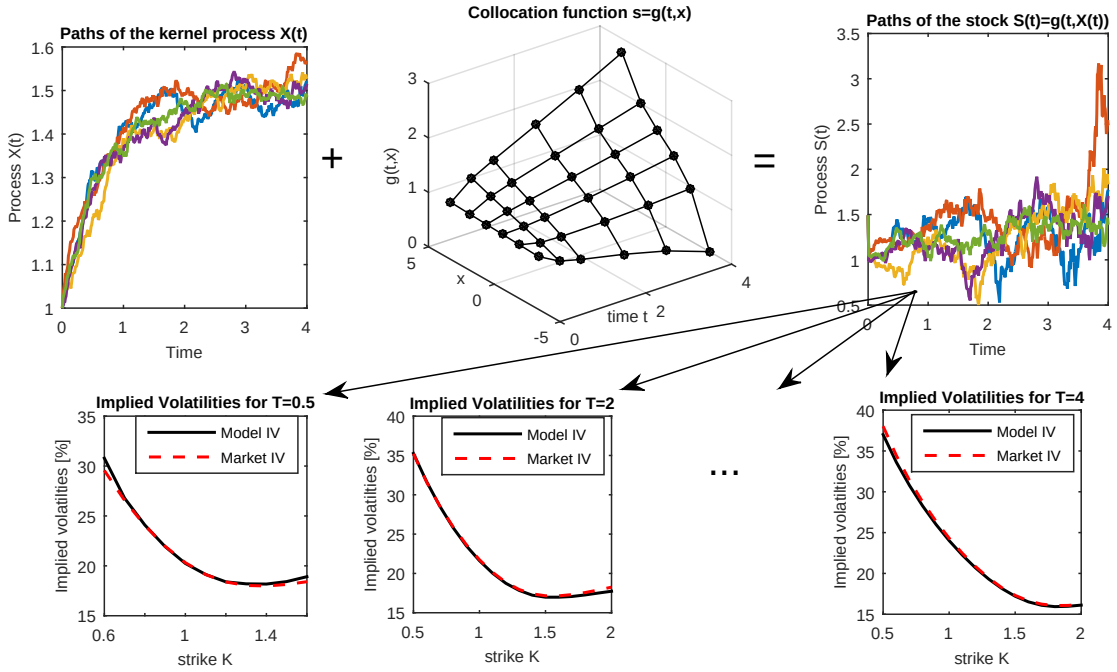

Figure 4.1: The CLV model in a Monte Carlo simulation framework.

We explain the concept in more detail by considering an up-out put option – for other single barrier products similar results hold. Defining $S(\cdot)$ as the underlying, the price at t_0 of an up-out put option with strike K, barrier B, starting time t_0 and time to maturity T is given by:

$$V_{\text{UO-Put}}(t_0,T,K) := \frac{M_d(t_0)}{M_d(T)}\mathbb{E}^{\mathbb{Q}}\left[(K-S(T))^+ \mathbb{1}\left(\max_{t\in[t_0,T]} S(t) < B\right)\middle| \mathcal{F}(t_0)\right], \tag{4.1}$$

with $M_d(\cdot)$ defined as the domestic money account. As for the CLV framework $S(t) = g_N(t,X(t))$, we have

$$\begin{aligned} V_{\text{UO-Put}}(t_0,T,K) &= \frac{M_d(t_0)}{M_d(T)}\mathbb{E}^{\mathbb{Q}}\left[(K-g_N(T,X(T)))^+ \mathbb{1}\left(\max_{t\in[t_0,T]} (g_N(t,X(t)) < B\right)\middle| \mathcal{F}(t_0)\right] \\ &= \frac{M_d(t_0)}{M_d(T)}\mathbb{E}^{\mathbb{Q}}\left[(K-g_N(T,X(T)))^+ \mathbb{1}\left(\max_{t\in[t_0,T]} (X(t) < g_N^{-1}(B)\right)\middle| \mathcal{F}(t_0)\right], \end{aligned}$$

where we employ the fact that by construction $g_N(\cdot,\cdot)$ is a monotone function.

Defining

$$\overline{B} := g_N^{-1}(B),$$

we write the option value – suppressing the discounting, the $\mathbb{Q}$-superscript and filtration, for notation purposes – as follows:

$$\begin{aligned} V_{\text{UO-Put}}(t_0,T,K) &= \mathbb{E}\left[\mathbb{E}\left[(K-g_N(T,X(T)))^+ \mathbb{1}\left(\max_{t\in[t_0,T]} X(t) < \overline{B}\right)\middle| X(t_0),X(T)\right]\right] \\ &= \mathbb{E}\left[(K-g_N(T,X(T)))^+ \cdot \left(1-\mathbb{Q}\left(\max_{t\in[t_0,T]} X(t) \geq \overline{B}\middle| X(t_0),X(T)\right)\right)\right]. \end{aligned}$$

We are interested in the probability

$$\mathbb{Q}\left(\max_{t\in[t_0,T]} X(t) \geq \overline{B}\middle| X(t_0),X(T)\right), \tag{4.2}$$

i.e. the probability that the maximum of $X(\cdot)$ on $[t_0, T]$ hits or crosses $\overline{B}$, given $X(t_0)$ and $X(T)$[11]. In the following, we explain how this *conditional hitting probability* can be approximated.

Given a general one-dimensional process under the $\mathbb{Q}$-measure:

$$\mathrm{d}X(t) = a(X(t))\mathrm{d}t + b(X(t))\mathrm{d}W^{\mathbb{Q}}(t),\ X_0 := X(0).$$

For simulating this process we use the Euler discretization

$$\widehat{X}_{k+1,m} = \widehat{X}_{k,m} + a(\widehat{X}_{k,m})\Delta + b(\widehat{X}_{k,m})(W_{k+1,m} - W_{k,m}), \tag{4.3}$$

with $k = 0, \ldots, K-1$ and $m = 1, \ldots, \mathcal{M}$ indicating the time-step and path, respectively, and $\Delta := T/K$, $\widehat{X}_0 := X_0$, $\widehat{X}_k := \widehat{X}(t_k)$, with $t_k = k\Delta$.

Result 4.1 (Simulation of the maximum)**.** *Given the values $\widehat{X}_{k,m}$ and $\widehat{X}_{k+1,m}$, the maximum*

$$\overline{X}_{k,m} := \max_{t\in[t_k,t_{k+1}]} \widehat{X}(t)$$

can be simulated by

$$\overline{X}_{k,m} = \frac{1}{2}\left(\widehat{X}_{k+1,m} + \widehat{X}_{k,m} + \sqrt{\left(\widehat{X}_{k+1,m} - \widehat{X}_{k,m}\right)^2 - 2b^2(\widehat{X}_{k,m})\Delta\log(U_{k,m})}\right), \tag{4.4}$$

with $U_{k,m} \overset{\mathrm{d}}{=} \mathcal{U}[0,1]$ being independent across the time-steps. A step to arrive at (4.4) is that

$$\{X(t),\ t_k \le t \le t_{k+1}\}$$

is approximated by an arithmetic Brownian motion with constant parameters $a(\widehat{X}_{k,m})$ and $b(\widehat{X}_{k,m})$. Conditional on the endpoint $X(t_{k+1})$, $\{X(t),\ t_k \le t \le t_{k+1}\}$ is a Brownian bridge.

Using (4.4) in Result 4.1, one can compute the probability that the discretized process hits the barrier $\overline{B}$ in the kth step, conditional on the values of $\widehat{X}_{k,m}$ and $\widehat{X}_{k+1,m}$. Straightforward calculus yields

$$\begin{aligned}
&\mathbb{Q}\left(\overline{X}_{k,m} \ge \overline{B} \middle| \widehat{X}_{k,m},\ \widehat{X}_{k+1,m}\right) \\
&= \begin{cases} 1 & \text{if } \widehat{X}_{k,m} \ge \overline{B} \text{ and/or } \widehat{X}_{k+1,m} \ge \overline{B}, \\ \exp\left(-\frac{2}{b^2(\widehat{X}_{k,m})\Delta}(\widehat{X}_{k,m} - \overline{B})(\widehat{X}_{k+1,m} - \overline{B})\right) & \text{if } \widehat{X}_{k,m} < \overline{B} \text{ and } \widehat{X}_{k+1,m} < \overline{B}. \end{cases}
\end{aligned} \tag{4.5}$$

Applying the discretization scheme in (4.3), the conditional hitting probability in (4.2) can be approximated by

$$\begin{aligned}
\mathbb{Q}\left(\max_{t\in[t_0,T]} X(t) \ge \overline{B} \middle| X(t_0), X(T)\right) &= 1 - \mathbb{Q}\left(\max_{t\in[t_0,T]} X(t) < \overline{B} \middle| X(t_0), X(T)\right) \\
&\approx 1 - \prod_{k=0}^{K-1}\left\{1 - \mathbb{Q}\left(\overline{X}_{k,m} \ge \overline{B} \middle| \widehat{X}_{k,m},\ \widehat{X}_{k+1,m}\right)\right\},
\end{aligned}$$

with $\mathbb{Q}\left(\overline{X}_{k,m} \ge \overline{B} \middle| \widehat{X}_{k,m},\ \widehat{X}_{k+1,m}\right)$ given in (4.5). Substituting this result in (4.2) yields:

$$\begin{aligned}
V_{\text{UO-Put}} &\approx \frac{M_d(t_0)}{M_d(T)}\mathbb{E}^{\mathbb{Q}}\Big[(K - g_N(T, X(T)))^+ \cdot \prod_{k=0}^{K-1}\left\{1 - \mathbb{Q}\left(\overline{X}_k \ge \overline{B} \middle| \widehat{X}_k,\ \widehat{X}_{k+1}\right)\right\}\Big] \\
&= \frac{1}{\mathcal{M}}\frac{M_d(t_0)}{M_d(T)}\sum_{m=1}^{\mathcal{M}}\left[\left(K - g_N\left(T, \widehat{X}_{K,m}\right)\right)^+ \prod_{k=0}^{K-1}\left\{1 - \mathbb{Q}\left(\overline{X}_{k,m} \ge \overline{B} \middle| \widehat{X}_{k,m},\ \widehat{X}_{k+1,m}\right)\right\}\right],
\end{aligned} \tag{4.6}$$

with $\mathbb{Q}\left(\overline{X}_{k,m} \ge B \middle| \widehat{X}_{k,m},\ \widehat{X}_{k+1,m}\right)$ given in (4.5). In the calibration of the CLV model to continuously monitored barrier options we make use of the expression in equation (4.6).

[11] Trivially, if $X(t_0) \ge \overline{B}$ and/or $X(T) \ge \overline{B}$, this probability is 1.

4.3 Calibration of the OU-CLV, CIR-CLV and Heston-CLV models to FX barrier options

In this section we calibrate the OU-CLV, CIR-CLV and Heston-CLV models to continuously monitored FX barrier option prices. In particular, for these 3 models we perform the following 2 steps:

1. **Calibration:** given a particular kernel process, calibrate the relevant kernel parameter(s) to market barrier option prices by Monte Carlo simulation[12]. The Monte Carlo simulation runs consist of 10 time-steps per year and we employ the Brownian bridge technique described in Section 4.2 – in particular, we use the result in equation (4.6).

2. **Pricing:** given the calibrated kernel parameter values, price the up-out put options by a standard Monte Carlo procedure of the CLV model with 250 time-steps per year to determine the calibration error, which is defined as

$$\epsilon := \sum_{i=1}^{N} |V_i - V_i^{\text{CLV}}|, \tag{4.7}$$

   with V_i and V_i^{CLV} denoting the mid-market price and the CLV price of the ith up-out put option, respectively, and N is the number of barrier options we calibrate to.

We consider USD/AUD FX market prices quoted on 12 June 2013 from a market data vendor. Domestic currency is USD, foreign currency is AUD. Initial spot is $S_0 = 0.9548$. The dataset consists of 7 expiries, namely 0.5, 0.75, 1, 2, 3, 4 and 5 years. For each expiry 5 implied volatility quotes are given, of which the middle (third) one is the ATM volatility. We calibrate to 9 continuously monitored *up-out put options* with different barrier and strike values, of which the price is given by (4.1).

For all three kernel process choices (OU, CIR and Heston) we compute $x_{i,j}$ and $s_{i,j}$ values for the expiries 1/365, 2/365, 3/365, 4/365, 1/52, 2/52, 1/12, 1/6, 1/4, 1/2, 3/4, 1 and 2, for which market volatility quotes are available[13]. In both the calibration and in the pricing afterwards we use $1 \cdot 10^4$ paths[14]. The target function is defined as the sum of squared errors of the 9 barrier options together, where the error is defined as the difference between the model and mid market prices.

4.3.1 The OU-CLV model

In Section 3.1 we observed that only the mean reversion parameter κ of the OU-CLV model affects the shape of the forward smile. Therefore, we calibrate κ and the other parameters are set to $X_0 = 1,\ \theta = 0.1,\ \gamma = 0.25$, which were just chosen values in [21]. Further, we use 6 collocation points. In the calibration we price for 20 'κ candidates' -1, -0.9, ..., 0.9, 1 (excluding $\kappa = 0$) up-out put options by (4.6) in a Monte Carlo simulation.

The calibration results in $\kappa = 0.1$ ***and takes*** 8 ***seconds***[15]**.** Results are displayed in Table 4. Two barrier option prices are outside the bid-ask spread. By construction, the OU-CLV model calibrates perfectly to European-type options – in Figure 4.2 we display the implied volatilities corresponding to 3M, 1Y and 2Y corresponding to the market, market parameterization and the OU-CLV model.

[12] The target function value is $\sum_{i=1}^{N} \left(V_i - V_i^{\text{CLV}}\right)^2$, with V_i and V_i^{CLV} denoting the mid-market price and the CLV price of the ith up-out put option, respectively, and N is the number of barrier options we calibrate to.

[13] We use a SABR market parameterization.

[14] In fact, we use 10 seeds with each seed constituting 10^3 paths. For the OU-CLV case we apply antithetic sampling, i.e. per seed we use $5 \cdot 10^2$ paths and $5 \cdot 10^2$ 'antithetic paths'.

[15] Processor: Intel(R) Core(TM) i7-4790 CPU @ 3.60GHz, 3601 Mhz, 4 Core(s), 8 Logical Processor(s). Available Physical Memory is 9.08 GB of in total 16 GB. Simulated with MATLAB.

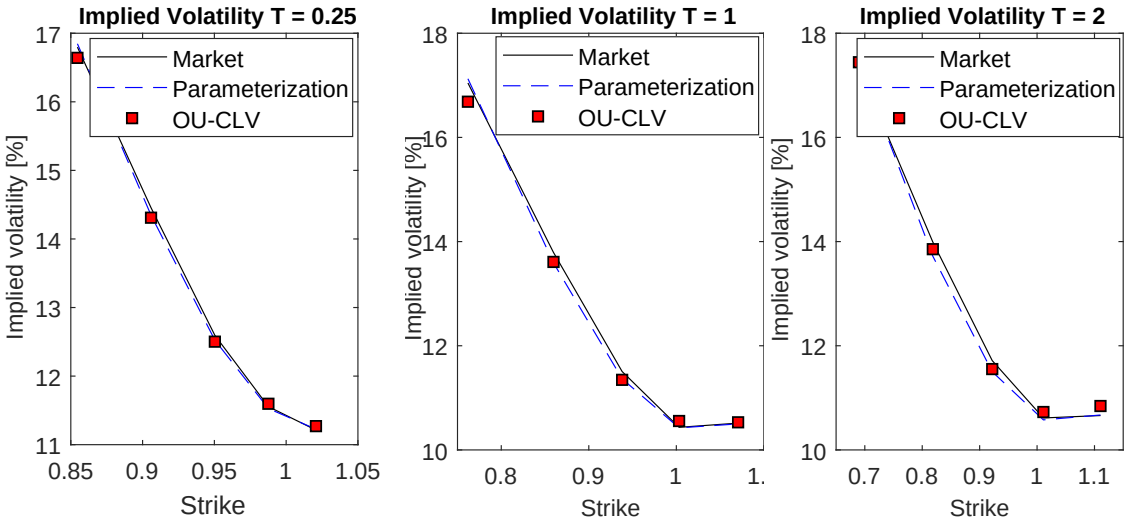

Figure 4.2: Implied volatilities corresponding to the OU-CLV model with $\kappa = -0.1$, $X_0 = 1$, $\theta = 0.1$, $\gamma = 0.25$.

4.3.2 The CIR-CLV model

In the CIR-CLV model, parameter γ has the most pronounced curvature effect, see Section 3.2.2. It also has a level effect. We therefore calibrate γ and leave the other parameters fixed, namely $\kappa = 0.1$, $\theta = 0.1$ and $X_0 = 1$. In the calibration we price for 20 'γ candidates' on a uniform grid between 0.1 and 1 up-out put options by (4.6) in a Monte Carlo simulation.

The calibration results in $\gamma = 0.526$ ***and takes*** 39 ***seconds***[15]***.***[16] Results are displayed in Table 4. Two barrier option prices are outside bid-ask spread. The calibration accuracy may be further enhanced by calibrating an additional parameter. *Additionally, we obtain an accurate calibration to the European-type options by construction, similar to the results in Figure 4.2 for the OU-CLV model.*

4.3.3 The Heston-CLV model

As we observed in Section 3.3.3, the mean reversion κ, volatility of variance γ and long-term variance $\overline{v}$ have a curvature effect – see also Table 3. As the curvature effect of γ is most pronounced, we calibrate γ and fix κ and $\overline{v}$. Assuming κ to be constant is justified by observations in [17], where it is argued that the effect on the implied volatility surface of increasing κ is similar to decreasing γ. Besides for $\overline{v}$, the only parameter having a skewness effect is $\rho_{x,v}$. We therefore also calibrate $\rho_{x,v}$. Last, v_0 has a level effect. We can already achieve an accurate level fit *a priori* by setting $v_0 = \overline{\sigma}^2_{\text{mkt}}(K_{\text{ATM}}, T_{\min})$, with $T_{\min} = 1/365$ and $\overline{\sigma}_{\text{mkt}}(K,t)$ denoting the market implied volatility corresponding to strike K and expiry t. The other fixed parameter values are $\kappa = 0.3$, $X_0 = 1$, $v_0 = \overline{\sigma}^2_{\text{mkt}}(K_{\text{ATM}}, T_{\min}) = 0.0625$, with $T_{\min} = 1/365$ and $\overline{v} = \overline{\sigma}^2_{\text{mkt}}(K_{\text{ATM}}, T_{\max}) = 0.0137$, with $T_{\max} = 2$. We use $N = 6$ collocation points.

In the calibration we choose 5 γ and 5 $\rho_{x,v}$ candidates uniformly between 0.1 and 1 and -1 and 0, respectively – so in total we consider 25 $(\gamma, \rho_{x,v})$-pairs. For each of the 25 pairs we price the up-out put options by (4.6) in a Monte Carlo simulation.

The calibration results in $\gamma = 0.1$ ***and*** $\rho_{x,v} = 0$ ***and takes*** 16 ***seconds***[15]***.*** Results are displayed in Table 4. One barrier option price is outside bid-ask spread. The total calibration error (4.7) is smaller than for the OU-CLV and CIR-CLV models. The reason

[16] This calibration is relatively slow compared to the calibration of the OU-CLV and Heston-CLV models. The reason is that the MATLAB functionality `ncx2cdf(x,d,λ)` is relatively slow for a large value of `x` (in fact we divide by a small $c(T_i)$ value, see (3.8)) and $\lambda(T_i)$ values, which is the case for the shortest T_i expiries.

Expiry	Barrier	Strike	OU-CLV	CIR-CLV	Heston-CLV
3M	1	0.9	97.2	88.8*	96.3
3M	1	0.85	36.8	26.0*	35.4
3M	0.97	0.9	67.3*	60.3	64.3*
1Y	1	0.8	99.2	92.9	98.7
1Y	1	0.85	161.2	157.9	162.1
1Y	0.97	0.8	50.8	50.8	52.3
2Y	1	0.75	128.4	132.0	147
2Y	1.05	0.7	109.5*	121.7	131.1
2Y	0.97	0.75	53.6	61.9	66.4
Calibration error ϵ			**53.9**	**38.4**	**33.5**
Calibration time[15]			**8s**	**39s**	**16s**

Table 4: Pricing up-out put options with the OU-CLV, CIR-CLV and Heston-CLV models after the calibration. The Monte Carlo simulation consists of 10^4 paths and 250 time-steps per year. ϵ is defined as the sum of absolute errors over the 9 barrier options, i.e. $\epsilon := \sum_{i=1}^{9} |V_i - V_i^{\text{CLV}}|$, with V_i and V_i^{CLV} denoting the mid-market price and the CLV price of the ith up-out put option, respectively. The red values marked by an asterisk (*) are not within bid-ask spread.

is that the Heston kernel process is *richer*; compared to the OU-CLV and CIR-CLV model, the Heston-CLV model is more flexible in capturing the forward smile, and as such in the calibration to forward volatility sensitive products, like barrier options. The calibration accuracy may be further enhanced by calibrating an additional parameter.

5 Conclusion

In this article we discussed a competitive alternative to stochastic-local volatility models, namely the Collocation Local Volatility (CLV) model, introduced in [21]. In the CLV model the local volatility function, based on stochastic collocation [2, 16, 39, 40, 40], connects a relatively simple and easy to implement kernel process to the market, resulting in a perfect calibration to liquid market quotes. The local volatility function only needs to be evaluated at the time-points of interest, e.g. the monitoring dates of a discrete barrier option. Moreover, efficient simulation schemes for the kernel process exist. Further, a proper choice of the kernel process allows the CLV model to be flexible to 'capture' the forward smile and, as such, price path-dependent products.

As the CLV model is sufficiently flexible in controlling the forward smile and can be efficiently evaluated, it allows for a rapid calibration to exotic options, while the fit to European-type options is preserved. In Section 4 we employ Brownian bridge techniques to calibrate the kernel process to continuously monitored barrier options in an efficient way; the calibration of the Heston-CLV model to the barrier options costs 16 seconds.

Based on the calibration results in Section 4, we prefer the Heston-CLV model for the calibration to continuously monitored path-dependent options. Its calibration is reasonably fast and yields the smallest calibration error; the reason is that among the kernel processes considered, the Heston kernel process allows for the most flexibility in capturing the forward smile. Further, for the Heston model low-bias large time-stepping Monte Carlo schemes exist, e.g. Andersen's QE scheme [1], which can be employed for the simulation of the Heston kernel.

In the case that we are interested in an exotic option monitored on a coarse grid, the CIR-CLV model may be preferred. Brownian bridge techniques are not needed as the CIR kernel process allows for large time-steps. For example, for the pricing of forward-start options in Section 3.2.2 the Monte Carlo simulation merely consists of 2 time-steps per year.

Additionally, the CIR parameters allow for controlling the level and the curvature of the forward smile, see Section 3.2.2.

In terms of simplicity and calibration speed (to exotics), the OU-CLV model outperforms the CIR-CLV and Heston-CLV models. In the OU-CLV model only the mean-reversion parameter κ has an effect on the forward volatility. As analytical expressions for its moments are available and the moments are numerically stable, we can compute optimal collocation points. Similar to the CIR-CLV model, the OU-CLV model allows for large time-steps.

References

[1] L. Andersen. Simple and Efficient Simulation of the Heston Stochastic Volatility Model. *Journal of Computational Finance*, 11(3):1–42, 2008.

[2] I. Babuška, F. Nobile, and R. Tempone. A Stochastic Collocation Method for Elliptic Partial Differential Equations with Random Input Data. *SIAM Journal on Numerical Analysis*, 45(3):1005–1034, 2007.

[3] G. Baker, R. Beneder, and A. Zilber. FX Barriers with Smile Dynamics. *Available at SSRN 964627*, 2004.

[4] P. Baldi. Exact asymptotics for the probability of exit from a domain and applications to simulation. *The Annals of Probability*, pages 1644–1670, 1995.

[5] J. Beck, R. Tempone, F. Nobile, and L. Tamellini. On the Optimal Polynomial Approximation of Stochastic PDEs by Galerkin and Collocation Methods. *Mathematical Models and Methods in Applied Sciences*, 22(09):1–33, 2012.

[6] M. Broadie and Ö. Kaya. Exact Simulation of Stochastic Volatility and Other Affine Jump Diffusion Processes. *Operations Research*, 54(2):217–231, 2006.

[7] R. H. Cameron and W. T. Martin. The Orthogonal Development of Non-Linear Functionals in Series of Fourier-Hermite Functionals. *Annals of Mathematics*, 48(2):385–392, 1947.

[8] P. Carr and D. Madan. Option Valuation using the Fast Fourier Transform. *Journal of Computational Finance*, 2(4):61–73, 1999.

[9] I. J. Clark. *Foreign Exchange Option Pricing: A Practitioners Guide*. John Wiley & Sons, 2011.

[10] E. Derman, D. Ergener, and I. Kani. Static Options Replication. *The Journal of Derivatives*, 2(4):78–95, 1995.

[11] E. Derman and I. Kani. Stochastic Implied Trees: Arbitrage Pricing with Stochastic Term and Strike Structure of Volatility. *International Journal of Theoretical and Applied Finance*, 1(1):61–110, 1998.

[12] B. Dupire. Pricing With a Smile. *Risk Magazine*, 7(1):18–20, 1994.

[13] F. Fang and C. W. Oosterlee. A Novel Pricing Method for European Options Based on Fourier-Cosine Series Expansions. *SIAM Journal on Scientific Computing*, 31(2):826–848, 2008.

[14] J. Favard. Sur les polynomes de tchebicheff. *CR Acad. Sci. Paris*, 200:2052–2053, 1935.

[15] F. N. Fritsch and R. E. Carlson. Monotone Piecewise Cubic Interpolation. *SIAM Journal on Numerical Analysis*, 17(2):238–246, 1980.

[16] B. Ganapathysubramanian and N. Zabaras. Sparse Grid Collocation Schemes for Stochastic Natural Convection Problems. *Journal of Computational Physics*, 225(1):652–685, 2007.

[17] P. Gauthier and P.-Y. Rivaille. Fitting the Smile, Smart Parameters for SABR and Heston. *Available at SSRN 1496982*, 2009.

[18] P. Glasserman. *Monte Carlo Methods in Financial Engineering*, volume 53. Springer Science & Business Media, 2003.

[19] E. Gobet. Advanced Monte Carlo methods for barrier and related exotic options. *Handbook of Numerical Analysis*, 15:497–528, 2009.

[20] L. Grzelak, J. Witteveen, M. Suarez, and C. Oosterlee. The Stochastic Collocation Monte Carlo Sampler: Highly Efficient Sampling from "Expensive" Distributions. *Quantitative Finance, doi: 10.1080/14697688.2018.1459807*, 2018.

[21] L. A. Grzelak. The CLV Framework-A Fresh Look at Efficient Pricing with Smile. *Available at SSRN 2747541*, 2016.

[22] L. A. Grzelak and C. W. Oosterlee. From Arbitrage to Arbitrage-Free Implied Volatilities. *Journal of Computational Finance*, 20(3):31–49, 2016.

[23] P. S. Hagan, D. Kumar, A. S. Lesniewski, and D. E. Woodward. Managing Smile Risk. *Wilmott Magazine*, pages 84–108, 2002.

[24] S. L. Heston. A Closed-Form Solution for Options with Stochastic Volatility with Applications to Bond and Currency Options. *The Review of Financial Studies*, 6:327–343, 1993.

[25] A. Janek, T. Kluge, R. Weron, and U. Wystup. FX smile in the Heston model. In *Statistical Tools for Finance and Insurance*, pages 133–162. Springer, 2011.

[26] M. Jex, R. Henderson, and D. Wang. Pricing Exotics under the Smile. *Risk*, 12(11):72–75, 1999.

[27] A. Lipton. The Vol Smile Problem. *Risk*, 15(2):61–66, 2002.

[28] A. Lipton, A. Gal, and A. Lasis. Pricing of Vanilla and First-Generation Exotic Options in the Local Stochastic Volatility Framework: Survey and new Results. *Quantitative Finance*, 14(11):1899–1922, 2014.

[29] M. Musiela and M. Rutkowski. *Martingale Methods in Financial Modelling – Second Edition*. Springer, 1997.

[30] F. Nobile, R. Tempone, and C. G. Webster. A Sparse Grid Stochastic Collocation Method for Partial Differential Equations with Random Input Data. *SIAM Journal on Numerical Analysis*, 46(5):2309–2345, 2008.

[31] A. Pascucci and A. Mazzon. The Forward Smile in Local-Stochastic Volatility Models. *Available at SSRN*, 2015.

[32] V. Piterbarg. Time to Smile. *Risk*, 18(5):71–75, 2005.

[33] Y. Ren, D. Madan, and M. Q. Qian. Calibrating and Pricing with Embedded Local Volatility Models. *Risk*, 20(9):138–143, 2007.

[34] M. Sankaran. Approximations to the Non-central Chi-square Distribution. *Biometrika*, 50:199–204, 1963.

[35] S. Sankaran and A. L. Marsden. A Stochastic Collocation Method for Uncertainty Quantification and Propagation in Cardiovascular Simulations. *Journal of Biomechanical Engineering*, 133(3):031001, 2011.

[36] Y. Tian, Z. Zhu, G. Lee, F. Klebaner, and K. Hamza. Calibrating and Pricing with a Stochastic-Local Volatility Model. *The Journal of Derivatives*, 22(3):21–39, 2015.

[37] A. W. van der Stoep, L. A. Grzelak, and C. W. Oosterlee. The Heston Stochastic-Local Volatility Model: Efficient Monte Carlo Simulation. *International Journal of Theoretical and Applied Finance*, 17(7):1450045, 2014.

[38] R. Weron and U. Wystup. Heston's model and the smile. In *Statistical tools for finance and insurance*, pages 161–181. Springer, 2005.

[39] J. A. S. Witteveen and G. Iaccarino. Simplex Stochastic Collocation with Random Sampling and Extrapolation for Nonhypercube Probability Spaces. *SIAM Journal on Scientific Computing*, 34(2):A814–A838, 2012.

[40] D. Xiu and J. S. Hesthaven. High-Order Collocation Methods for Differential Equations with Random Inputs. *SIAM Journal on Scientific Computing*, 27(3):1118–1139, 2005.

A Optimal collocation points

One of the relevant theorems with respect to computing optimal collocation points is the following [14]:

Theorem A.1 (Recurrence in orthogonal polynomials)**.** *For any given density function $f_X(\cdot)$, a unique sequence of monic orthogonal polynomials $p_i(x)$ exists, with deg$(p_i(x)) = i$, which can be constructed by*

$$p_{i+1}(x) = (x - \alpha_i)p_i(x) - \beta_i p_{i-1},\ i = 0, 1, \ldots, N-1,$$

with $p_{-1}(x) \equiv 0,\ p_0(x) \equiv 1$ and the recurrence coefficients

$$\alpha_i = \frac{\mathbb{E}\left[Xp_i^2(X)\right]}{\mathbb{E}\left[p_i^2(X)\right]},\ i = 0, 1, \ldots, N-1,\ \ \beta_i = \frac{\mathbb{E}\left[p_i^2(X)\right]}{\mathbb{E}\left[p_{i-1}^2(X)\right]},\ i = 1, 2, \ldots, N-1,$$

with $\beta_0 = 0$.

Proof. For a proof, see [14]. □

The recurrence coefficients α_i and β_i can be obtained via the moments of X. In particular, one can express the first N coefficients in terms of the elements of a lower triangular matrix R, which is obtained by the Cholesky decomposition of a matrix $M = R^T R$ that constitutes the first $2N$ moments of X. Given the recurrence coefficients, the *optimal* collocation points $x_1,\ x_2, \ldots, x_N$ are the zeros of the orthogonal polynomial $p_N(x)$ and can be computed by an eigenvalue method. Based on this, the only requirement for X to be an appropriate kernel variable for which we can compute N collocation points, is the existence of the first $2N$ moments.

By choosing the collocation points as zeros of the orthogonal polynomial $p_N(\cdot)$ – see Theorem A.1 – the stochastic collocation method can be connected to the computation of integrals by Gauss quadrature, which for the function $\Psi(\cdot)$ (which is required to be well approximated by a polynomial function), weight function $f_X(\cdot)$ and quadrature weights ω_i, $i = 1, 2, \ldots, N$ reads:

$$\mathbb{E}\left[\Psi(X)\right] = \int_{\mathbb{R}} \Psi(x) f_X(x) \mathrm{d}x = \sum_{i=1}^{N} \Psi(x_i)\omega_i + \epsilon_N. \tag{A.1}$$

By choosing $\Psi(x) = (g(x) - g_N(x))^2$, with $g(\cdot) = F_S^{-1}(F_X(\cdot))$ and $g_N(\cdot)$ the approximating polynomial function, we have

$$\mathbb{E}\left[\left(g(X) - g_N(X)\right)^2\right] = \int_{\mathbb{R}} (g(x) - g_N(x))^2 f_X(x) \mathrm{d}x = \sum_{i=1}^{N} (g(x_i) - g_N(x_i))\omega_i + \epsilon_N = \epsilon_N, \tag{A.2}$$

since $g(x_i) = g_N(x_i)$, $i = 1, 2, \ldots, N$. So, in L^2 the error is determined by the quadrature error. Further, when choosing e.g. X to be the standard normal distribution, a simple linear relation between the stochastic collocation pairs (x_i, ω_i) and the Gauss-Hermite quadrature pairs (x_i^H, ω_i^H) exists.

B The CLV pricing PDE: alternative proof

In this appendix we provide an alternative proof for Lemma 2.2, which is based on a replicating portfolio approach. To express the PDE merely in terms of derivatives to X, we define

$$\widetilde{V}(t, X(t)) := V(t, g_N(t, X(t))) = V(t, S(t)), \tag{B.1}$$

with $V(t, S(t))$ representing the value of a European option on the underlying $S(\cdot)$ ('plain vanilla contingent claim').

Lemma B.1 (CLV pricing PDE)**.** *Given the CLV model under the risk-neutral $\mathbb{Q}$-measure with a general one-dimensional kernel process $X(\cdot)$:*

$$\begin{aligned} S(t) &= g_N(t, X(t)), \\ \mathrm{d}X(t) &= \mu^{\mathbb{Q}}(t, X(t))\mathrm{d}t + \sigma(t, X(t))\mathrm{d}W^{\mathbb{Q}}(t). \end{aligned}$$

Suppose that the partial derivatives of $g_N := g_N(t, X(t))$, $\partial g_N/\partial X$, $\partial^2 g_N/\partial X^2$ and $\partial g_N/\partial t$ exist. Also, assume that the money account $M(\cdot)$ is determined by $\mathrm{d}M(t) = rM(t)\mathrm{d}t$, with r denoting a constant interest rate. Then $\widetilde{V} := \widetilde{V}(t, X(t))$ defined in (B.1) is governed by

$$\frac{\partial \widetilde{V}}{\partial t} + \mu^{\mathbb{Q}}(t, X)\frac{\partial \widetilde{V}}{\partial X} + \frac{1}{2}\sigma^2(t, X)\frac{\partial^2 \widetilde{V}}{\partial X^2} - r\widetilde{V} = 0,$$

with the final condition

$$\widetilde{V}(T, X(T)) = \Phi(g_N(T, X(T))),$$

where $\Phi(\cdot)$ is a payoff function depending on the final state of $g_N(\cdot, \cdot)$.

Proof. We start with the CLV model, under the *real-world* $\mathbb{P}$-measure:

$$\begin{aligned} S(t) &= g_N(t, X(t)), \\ \mathrm{d}X(t) &= \mu^{\mathbb{P}}(t, X(t))\mathrm{d}t + \sigma(t, X(t))\mathrm{d}W^{\mathbb{P}}(t). \end{aligned}$$

Suppressing the arguments of $g_N(t, X(t))$, assuming that the partial derivatives $\partial g_N/\partial X$, $\partial^2 g_N/\partial X^2$ and $\partial g_N/\partial t$ exist, $S(\cdot)$ follows an Itô process which is governed by the same Wiener process as $X(\cdot)$ and reads:

$$\mathrm{d}S(t) = \left(\frac{\partial g_N}{\partial t} + \mu^{\mathbb{P}}(t, X(t))\frac{\partial g_N}{\partial X} + \frac{1}{2}\frac{\partial^2 g_N}{\partial X^2}\sigma^2(t, X(t))\right)\mathrm{d}t + \frac{\partial g_N}{\partial X}\sigma(t, X(t))\mathrm{d}W^{\mathbb{P}}(t).$$

By Itô's lemma, introducing the short-hand notation $V := V(t, S(t))$, we obtain the dynamics of the European option $V(t, S(t))$:

$$\begin{aligned} \mathrm{d}V(t, S(t)) &= \left[\frac{\partial V}{\partial t} + \frac{\partial V}{\partial S}\left(\frac{\partial g_N}{\partial t} + \mu^{\mathbb{P}}(t, X(t))\frac{\partial g_N}{\partial X} + \frac{1}{2}\frac{\partial^2 g_N}{\partial X^2}\sigma^2(t, X(t))\right)\right. \\ &\quad \left. + \frac{1}{2}\frac{\partial^2 V}{\partial S^2}\left(\frac{\partial g_N}{\partial X}\right)^2\sigma^2(t, X(t))\right]\mathrm{d}t + \frac{\partial V}{\partial S}\frac{\partial g_N}{\partial X}\sigma(t, X(t))\mathrm{d}W^{\mathbb{P}}(t). \quad \text{(B.2)} \end{aligned}$$

Analogously to the derivation of the standard Black-Scholes pricing PDE, we construct a replicating portfolio $\Pi(\cdot)$, which consists of $a(\cdot)$ stocks with value $S(\cdot)$ and $b(\cdot)$ units of the riskless bond $M(\cdot)$, which is determined by $\mathrm{d}M(t) = rM(t)\mathrm{d}t$, where r is the risk-free rate. Assuming the portfolio to be *self-financing*, i.e. the change in the value of the portfolio is only due to changes in the value of the underlying assets, and not due to inflows or outflows of funding, we have

$$\mathrm{d}\Pi(t) = a(t)\mathrm{d}S(t) + b(t)\mathrm{d}M(t).$$

By applying Itô's lemma, we derive its dynamics:

$$\begin{aligned} \mathrm{d}\Pi(t) &= \left[a(t)\left(\frac{\partial g_N}{\partial t} + \mu^{\mathbb{P}}(t, X(t))\frac{\partial g_N}{\partial X} + \frac{1}{2}\frac{\partial^2 g_N}{\partial X^2}\sigma^2(t, X(t))\right) + b(t)rM(t)\right]\mathrm{d}t \\ &\quad + a(t)\frac{\partial g_N}{\partial X}\sigma(t, X(t))\mathrm{d}W^{\mathbb{P}}(t). \quad \text{(B.3)} \end{aligned}$$

By observing the diffusion terms in equations (B.2) and (B.3), we easily see that $a(t) = \partial V/\partial S$. To determine $b(\cdot)$, we equate the drift terms of the portfolio (left-hand side) and the option (right-hand side):

$$\begin{aligned} &\frac{\partial V}{\partial S}\left(\frac{\partial g_N}{\partial t} + \mu^{\mathbb{P}}(t, X(t))\frac{\partial g_N}{\partial X} + \frac{1}{2}\frac{\partial^2 g_N}{\partial X^2}\sigma^2(t, X(t))\right) + b(t)rM(t) \\ &= \frac{\partial V}{\partial t} + \frac{\partial V}{\partial S}\left(\frac{\partial g_N}{\partial t} + \mu^{\mathbb{P}}(t, X(t))\frac{\partial g_N}{\partial X} + \frac{1}{2}\frac{\partial^2 g_N}{\partial X^2}\sigma^2(t, X(t))\right) + \frac{1}{2}\frac{\partial^2 V}{\partial S^2}\left(\frac{\partial g_N}{\partial X}\right)^2\sigma^2(t, X(t)). \end{aligned}$$

From this we obtain

$$b(t) = \frac{1}{rM(t)} \left[\frac{\partial V}{\partial t} + \frac{1}{2} \frac{\partial^2 V}{\partial S^2} \left(\frac{\partial g_N}{\partial X} \right)^2 \sigma^2(t, X(t)) \right].$$

Substituting the values for $a(\cdot)$ and $b(\cdot)$ yields

$$\Pi(t) = \frac{\partial V}{\partial S} S(t) + \frac{1}{r} \left[\frac{\partial V}{\partial t} + \frac{1}{2} \frac{\partial^2 V}{\partial S^2} \left(\frac{\partial g_N}{\partial X} \right)^2 \sigma^2(t, X(t)) \right].$$

The portfolio $\Pi(\cdot)$ and the option $V(\cdot)$ have the same cashflows, thus also – assuming the absence of arbitrage – the same value, implying

$$\frac{\partial V}{\partial t} + \frac{\partial V}{\partial S} rS(t) + \frac{1}{2} \frac{\partial^2 V}{\partial S^2} \left(\frac{\partial g_N}{\partial X} \right)^2 \sigma^2(t, X) - rV = 0. \tag{B.4}$$

We observe that the drift-term $\mu^{\mathbb{P}}(t, X(t))$ has vanished. To proceed, we derive an identity for $rS(t)$ by considering the dynamics of $S(\cdot)/M(\cdot)$ under the risk-neutral $\mathbb{Q}$-measure:

$$\mathrm{d}\left(\frac{S(t)}{M(t)} \right) = \frac{1}{M(t)} \left(\overline{\mu}^{\mathbb{Q}} - rS(t) \right) \mathrm{d}t + \frac{\partial g_N}{\partial X} \sigma(t, X(t)) \mathrm{d}W^{\mathbb{Q}}(t),$$

with

$$\overline{\mu}^{\mathbb{Q}} := \frac{\partial g_N}{\partial t} + \mu^{\mathbb{Q}}(t, X(t)) \frac{\partial g_N}{\partial X} + \frac{1}{2} \frac{\partial^2 g_N}{\partial X^2} \sigma^2(t, X(t)).$$

As $S(\cdot)/M(\cdot)$ is a martingale under the risk-neutral $\mathbb{Q}$-measure, the dt-term should be zero, i.e. $\overline{\mu}^{\mathbb{Q}} - rS(t) = 0$, or:

$$\frac{\partial g_N}{\partial t} + \mu^{\mathbb{Q}}(t, X) \frac{\partial g_N}{\partial X} + \frac{1}{2} \frac{\partial^2 g_N}{\partial X^2} \sigma^2(t, X) - r g_N(t, X) = 0.$$

By this condition, we write (B.4) as

$$\begin{aligned} &\frac{\partial V}{\partial t} + \frac{\partial V}{\partial S} \left(\frac{\partial g_N}{\partial t} + \mu^{\mathbb{Q}}(t, X) \frac{\partial g_N}{\partial X} + \frac{1}{2} \frac{\partial^2 g_N}{\partial X^2} \sigma^2(t, X) \right) \\ &\quad + \frac{1}{2} \frac{\partial^2 V}{\partial S^2} \left(\frac{\partial g_N}{\partial X} \right)^2 \sigma^2(t, X) - rV = 0. \end{aligned} \tag{B.5}$$

Using the notation (B.1) and the short-hand notations $V := V(t, S(t))$ and $\widetilde{V} := \widetilde{V}(t, X(t))$, we have

$$\frac{\partial V}{\partial S} = \frac{\partial \widetilde{V}}{\partial X} \frac{\partial X}{\partial S} \tag{B.6}$$

and also

$$\frac{\partial^2 V}{\partial S^2} = \frac{\partial}{\partial S} \left(\frac{\partial \widetilde{V}}{\partial X} \frac{\partial X}{\partial S} \right) = \left(\frac{\partial}{\partial S} \frac{\partial \widetilde{V}}{\partial X} \right) \frac{\partial X}{\partial S} + \frac{\partial \widetilde{V}}{\partial X} \frac{\partial^2 X}{\partial S^2} = \frac{\partial X}{\partial S} \frac{\partial^2 \widetilde{V}}{\partial X^2} \frac{\partial X}{\partial S} + \frac{\partial \widetilde{V}}{\partial X} \frac{\partial^2 X}{\partial S^2},$$

which we can write as

$$\frac{\partial^2 V}{\partial S^2} = \left(\frac{\partial X}{\partial S} \right)^2 \frac{\partial^2 \widetilde{V}}{\partial X^2} + \frac{\partial \widetilde{V}}{\partial X} \frac{\partial^2 X}{\partial S^2}. \tag{B.7}$$

As $\partial V/\partial t = \partial \widetilde{V}/\partial t$ and substituting the identities (B.6) and (B.7) in the PDE (B.5) yields

$$\begin{aligned} &\frac{\partial \widetilde{V}}{\partial t} + \frac{\partial \widetilde{V}}{\partial X} \left[\frac{\partial X}{\partial S} \frac{\partial g_N}{\partial t} + \mu^{\mathbb{Q}}(t, X) + \frac{1}{2} \sigma^2(t, X) \left(\frac{\partial X}{\partial S} \frac{\partial^2 g_N}{\partial X^2} + \frac{\partial^2 X}{\partial S^2} \left(\frac{\partial g_N}{\partial X} \right)^2 \right) \right] \\ &\quad + \frac{1}{2} \frac{\partial^2 \widetilde{V}}{\partial X^2} \sigma^2(t, X) - r\widetilde{V} = 0. \end{aligned}$$

The term multiplied by $\frac{1}{2}\sigma^2(t,X)$ equals zero, as for $X(t) = g_N^{-1}(g_N(t,X(t)))$ holds that:

$$\frac{\partial^2 X}{\partial S^2}\left(\frac{\partial S}{\partial X}\right)^2 + \frac{\partial X}{\partial S}\frac{\partial^2 S}{\partial X^2} = \left(\frac{\partial}{\partial X}\frac{\partial X}{\partial S}\right)\frac{\partial S}{\partial X} + \frac{\partial X}{\partial S}\frac{\partial^2 S}{\partial X^2} = \frac{\partial}{\partial X}\left(\frac{\partial X}{\partial S}\frac{\partial S}{\partial X}\right) = 0.$$

As such, the pricing PDE is:

$$\frac{\partial \widetilde{V}}{\partial t} + \left(\frac{\partial X}{\partial S}\frac{\partial g_N}{\partial t} + \mu^{\mathbb{Q}}(t,X)\right)\frac{\partial \widetilde{V}}{\partial X} + \frac{1}{2}\sigma^2(t,X)\frac{\partial^2 \widetilde{V}}{\partial X^2} - r\widetilde{V} = 0.$$

Assuming that the function $g_N(\cdot,\cdot)$ does not explicitly depend on t, we have $\partial g_N/\partial t = 0$ and we obtain the final result:

$$\frac{\partial \widetilde{V}}{\partial t} + \mu^{\mathbb{Q}}(t,X)\frac{\partial \widetilde{V}}{\partial X} + \frac{1}{2}\sigma^2(t,X)\frac{\partial^2 \widetilde{V}}{\partial X^2} - r\widetilde{V} = 0.$$

The final condition on $\widetilde{V}(\cdot)$ is given in terms of the payoff function $\Phi(\cdot)$ that depends on the final state of $g_N(\cdot,\cdot)$:

$$\widetilde{V}(T,X(T)) = \Phi(g_N(T,X(T))).$$

This concludes the proof of Lemma B.1. □

C Numerical experiment

We present a numerical experiment in which we perform the steps in Algorithm 1 to price a discretely monitored up-out call option:

$$V_{\text{UO-call}}(t_0,T,K) := \mathbb{E}^{\mathbb{Q}}\left[\frac{(S(T)-K)^+}{M(T)}\mathbb{1}(\max_{t\in\mathcal{T}} S(t) < B)\middle|\mathcal{F}(t_0)\right],$$

with $B = 1.5,\ K = 0.5,\ T = 3$ and quarterly monitoring dates, i.e. $\mathcal{T} = \{3\text{M}, 6\text{M}, \ldots, 3\text{Y}\}$. We use the Ornstein-Uhlenbeck CLV (OU-CLV) model

$$\begin{aligned} S(t) &= g_N(t,X(t)), \\ \mathrm{d}X(t) &= \kappa\left(\theta - X(t)\right)\mathrm{d}t + \gamma \mathrm{d}W^{\mathbb{Q}}(t),\ X(t_0) = X_0, \end{aligned}$$

with $X_0 = 1,\ \kappa = 1,\ \gamma = 0.5$ and $\theta = 0.5$. Given the filtration at $t_0 = 0$, the kernel variable $X(\cdot)$ is normally distributed with mean and variance as in (2.8).

We successively apply the steps of Algorithm 1:

1. We generate synthetic market data by the Heston model with the parameters $\kappa = 0.5,\ \gamma = 1,\ \rho_{x,v} = -0.7,\ v_0 = 0.04,\ \overline{v} = 0.04, r = 0$ and $S_0 = 1$. We assume that liquid market quotes are available for the expiries 1D, 2D, 3D, 4D, 1W, 2W, 1M, 2M, 3M, 6M, 9M, 1Y, 2Y, 3Y, 4Y and 5Y. In the left-hand plot of Figure C.1 the market-implied CDF is displayed, obtained by Fourier pricing techniques.

2. We use $N = 6$ collocation points. Given the optimal collocation points $z_j,\ j = 1,\ldots,N$ of a standard normal random variable $Z \overset{\mathrm{d}}{=} \mathcal{N}(0,1)$ (for $N = 6$ these are $-3,3243$, -1.8892, -0.6167, 0.6167, 1.8892, 3.3243), the optimal collocation points of $X(t)$ are given by $x_j(t) = \mathbb{E}\left[X(t)\right] + \sqrt{\mathbb{V}\mathrm{ar}[X(t)]}\cdot z_j$ [21] and as such

$$x_{i,j} := x_j(T_i) = \mathbb{E}\left[X(T_i)\right] + \sqrt{\mathbb{V}\mathrm{ar}[X(T_i)]}\cdot z_j,\ i = 1,\ldots,M,\ j = 1,\ldots,N.$$

   Given the collocation points, by inversion of the market-implied CDF we obtain the collocation values $s_{i,j} = F^{-1}_{S(T_i)}(F_{X(T_i)}(x_{i,j}))$. In the right-hand plot of Figure C.1 the triplets $(x_{i,j}, T_i, s_{i,j})$ are displayed.

3. We simulate the kernel variable with time-steps of 3 months (4 time-steps per year). The Monte Carlo simulation consists of $1 \cdot 10^4$ paths[17]. In order to evaluate $g_N(\cdot, \cdot)$ at time-points that are not part of the market data – so *not* 0.1, 0.25, 0.5, 1, 2, 3, 4 and 5 years – we interpolate between or extrapolate the $s_{i,j}$ values, see e.g. the interpolated $g_N(2.5, \cdot)$-values in the right-hand plot of Figure C.1.

4. Last, we price the up-out call option: $V_{\text{UO-call}}(t_0, T, K) = 0.4739$. The calibration to the European-type options is guaranteed to be almost perfect, see Figure C.2.

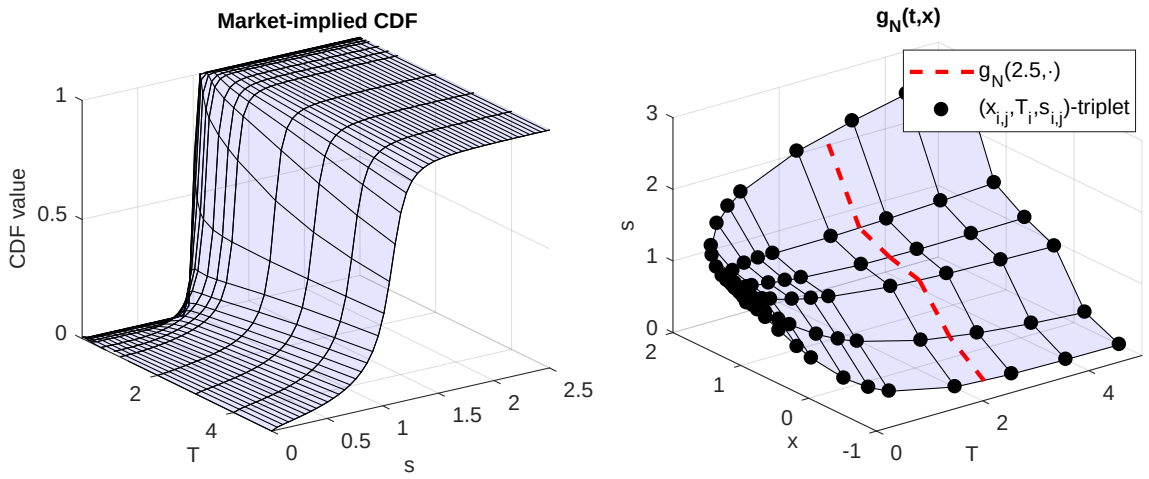

Figure C.1: The market-implied CDF (left) and the $(x_{i,j}, s_{i,j})$-pairs (right) corresponding to the numerical experiment in Appendix C. The red dashed line indicates the monotone interpolation at $t = 2.5$.

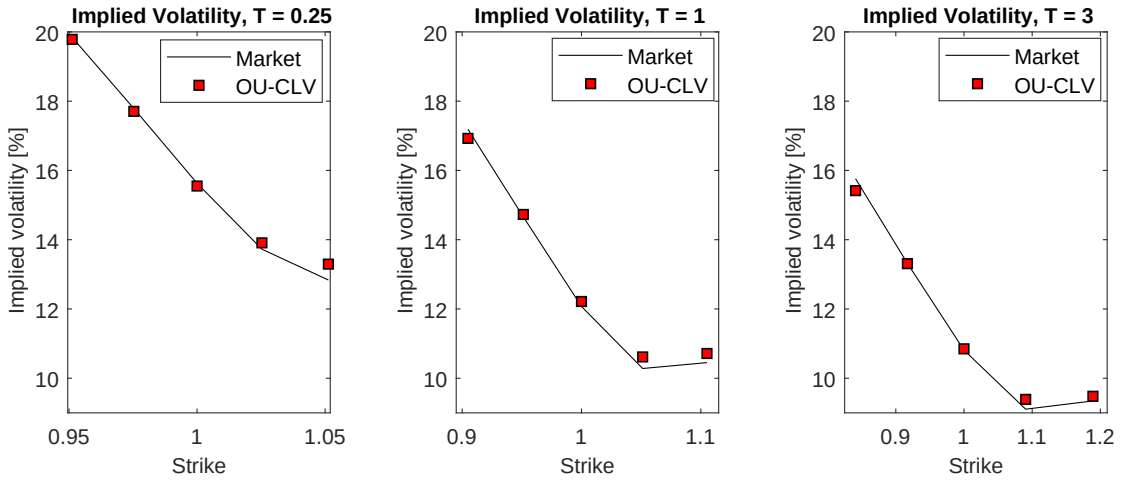

Figure C.2: The implied volatilities for the expiries $T = 0.25$, $T = 1$ and $T = 3$ corresponding to the numerical experiment in Appendix C.

D Effect of CIR parameters, omitting the level effect

In Figures D.1 and D.2 we display the effect of the CIR kernel parameters on the shape of the forward smile, see Section 3.2.2, but without the level effect.

[17] In fact, we use 10 seeds, each seed constitutes $1 \cdot 10^3$.

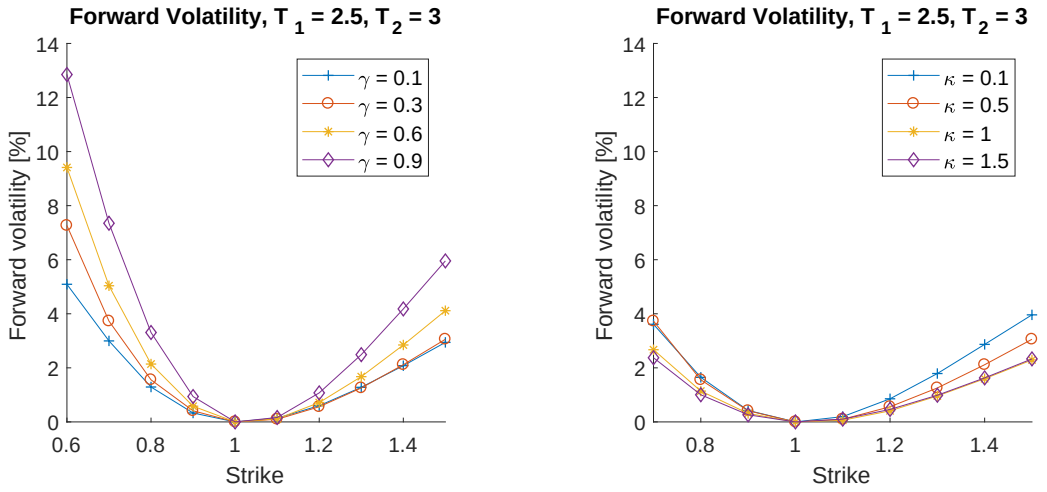

Figure D.1: Effect of γ (left) and κ (right) on the forward volatility smile for the CIR-CLV model, omitting the level effect, with $T_1 = 2.5$ and $T_2 = 3$. The 'base case' CIR parameters (if not varied) are: $\gamma = 0.3$, $\kappa = 0.5$, $\theta = 0.5$ and $X_0 = 1$.

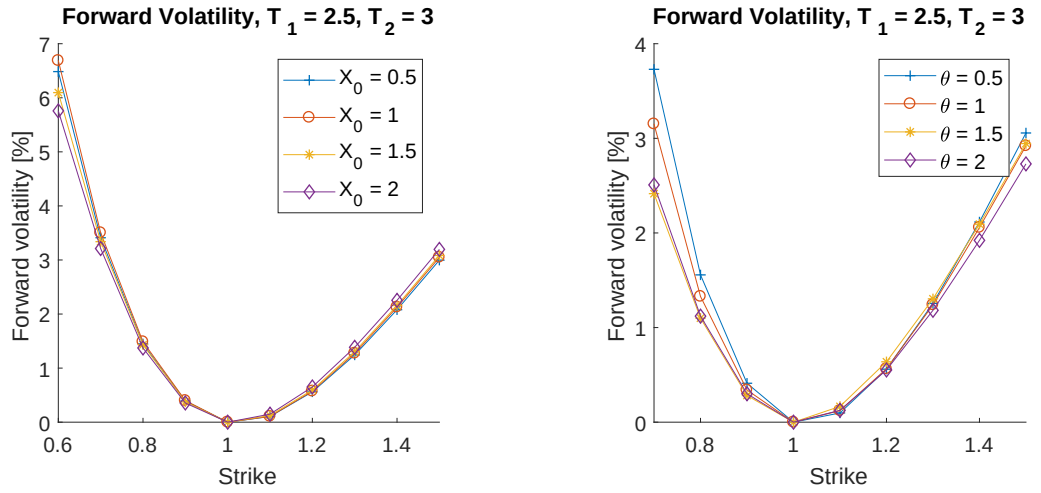

Figure D.2: Effect of X_0 (left) and θ (right) on the forward volatility smile for the CIR-CLV model, omitting the level effect, with $T_1 = 2.5$ and $T_2 = 3$. The 'base case' CIR parameters (if not varied) are: $\gamma = 0.3$, $\kappa = 0.5$, $\theta = 0.5$ and $X_0 = 1$.

E Effect of Heston parameters, omitting the level effect

In Figure E.1 we display the effect of γ and κ on the shape of the forward smile, see Section 3.3.3, but without the level effect. We do not display the effects of all parameters, to save some space.

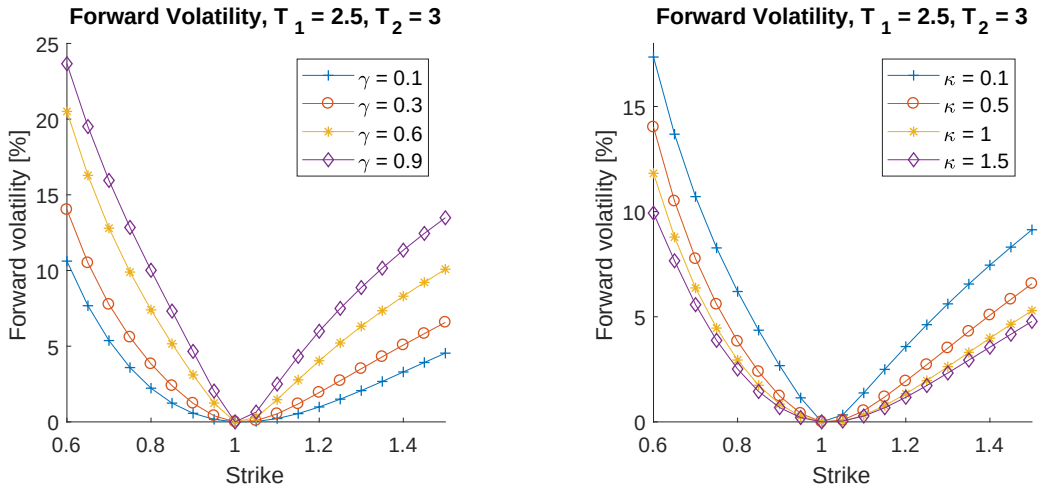

Figure E.1: Effect of γ (left) and κ (right) on the forward volatility smile for the Heston-CLV model, omitting the level effect, with $T_1 = 2.5$ and $T_2 = 3$. The 'base case' Heston parameters (if not varied) are: $\kappa = 0.5$, $\gamma = 0.3$, $\rho_{x,v} = 0$, $\overline{v} = 0.2$, $v_0 = 0.2$ and $X_0 = 1$.